CHALMERS

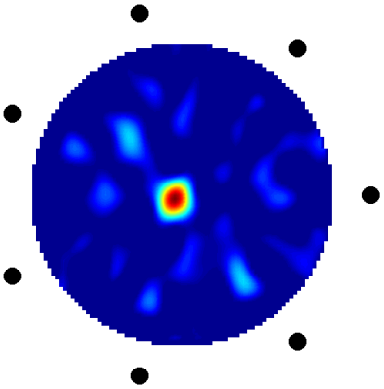

Regularization in Microwave Tomography

Alexey Voronov

Department of Signals and Systems

CHALMERS UNIVERSITY OF TECHNOLOGY

Göteborg, Sweden

EXE079/2007

Abstract

Microwave tomography is a promising method for the breast cancer imaging. Dielectric properties of the healthy tissue and the tumor have a high contrast under microwave investigation. To determine the dielectric properties from antenna measurements it is necessary to solve the inverse electromagnetic problem. This inverse problem is ill-posed, its solution is not stable. Regularization is used to achieve stability. Ordinary Tikhonov regularization usually makes the solution too smooth. Edge-preserving regularization is investigated to obtain a stable solution without oversmoothing the solution. Tikhonov and Edge-preserving regularizations are compared. It is found that edge-preserving regularization decreases the smoothness of the reconstruction but has the same robustness against the noise compared to Tikhonov regularization.

KEYWORDS: tomography, tissue properties, FDTD, optimization, regularization.

Contents

1 Introduction

Breast cancer is a serious problem in the modern world today. As reported by World Health Organization [1], it is the most common form of cancer in females. As much as one third of the women will get breast cancer during their lifetime. Early diagnostic is a key for a successful treatment. It is found by Michaelson et al [2], that survival rate is directly dependent on the size of the tumor when it was diagnosed. In diagnosing tumors imaging plays an important role. The most widespread imaging method today is x-ray imaging. Unfortunately this method has several disadvantages, such as that it uses ionizing radiation, that could potentially induce cancer in the patient. Another problem that the tumor has a relatively low contrast in the x-ray images in comparison to a normal tissue. The reason is that both normal and malignant tissues are soft tissues with similar attenuation of x-rays. Another disadvantage is uncomfortable breast compression during imaging. There are also other methods in use, for example ultrasound imaging and contrast-enhanced magnetic resonance imaging. They have their own advantages and disadvantages, e.g. price for MRI is very high. Microwave tomography has been suggested as an alternative due to its relatively low cost and high contrast in the dielectric properties between the healthy tissue and the tumor.

Dielectric properties of biological tissues has been studied for more than fifty years. A recent extensive survey was published by Gabriel et. al. [3, 4, 5]. Over the years it has been found in several studies ([6, 7, 8, 9, 10, 11, 12, 13, 14, 15]) that the dielectric properties of normal breast tissue differs greatly from the dielectric properties of cancerous tissue. Properties of the healthy tissue are close the properties of fat, while the tumor properties are closer to the properties of blood. Conductivity and relative permittivity for normal and malignant tissues over the interesting frequency band are presented in Figure 1.1 ([16][3, 4, 5][11, 15, 17, 14, 18, 13, 19]).

If it will be possible to determine the properties of a tissue from the microwave tomographic measurements, then it is also possible to predict if there is a tumor or not.

In tomographic measurements emitted wave propagates through the breast and the scattered field is measured by receivers. These measurements allow us to determine the dielectric properties of the breast. Algorithms for such inverse scattering generally fall into two broad categories: fast, approximate linear algorithms or slow, accurate non-linear algorithms. The linear algorithms usually based on inversion of the Fourier transform (e.g. Bertero et.al. [20]) or Born approximations (Bulyshev et.al. [21]). In contrast, nonlinear algorithms usually require some sort of computationally expensive Newton-like search (Gustafsson and He [22]). There are few options available in between, e.g. “linear sampling” method developed by Colton and Kirsch [23]. Comparison of linear

and non-linear algorithm has been done for breast cancer imaging by Fhager et. al. [24] and it was found that the linear algorithms are incapable to perform sufficiently good reconstruction due to high contrast between the healthy tissue and the tumor under microwave investigations. That is why a non-linear approach is used in this work.

The particular reconstruction algorithm used in this work can be outlined as follows. At first, the tissue properties are "guessed" and a simulation of the wave propagation is performed by solving the direct electromagnetic problem described in Section 2.1. Simulated data is compared to the measurements and the residual between them is taken as a measure of the misfit. Based on the residual a functional is defined which is minimized. Search methods for the minimization are described in Section 2.4. To update the reconstructed dielectric properties of the breast in each iteration of the minimization, gradients of the minimization functional are used. Derivation of the gradients has been described by, for example, Gustafsson [22]. The reconstruction problem is an inverse problems which is ill-posed. To solve ill-posed problems numerically, one must introduce some additional information about the solution, such as an assumption on the smoothness or a bound on the norm. A simple form of regularization, generally denoted Tikhonov regularization, is essentially a trade-off between fitting the data and reducing a norm of the solution. More recently, non-linear regularization methods have become popular. The purpose of this work is to investigate regularization methods and make comparison with Tikhonov regularization. Brief overview of several regularization methods in given in Section 2.5. Edge-preserving regularization is chosen for detailed investigation, and its derivation for microwave tomography is given in Section 2.5.6.

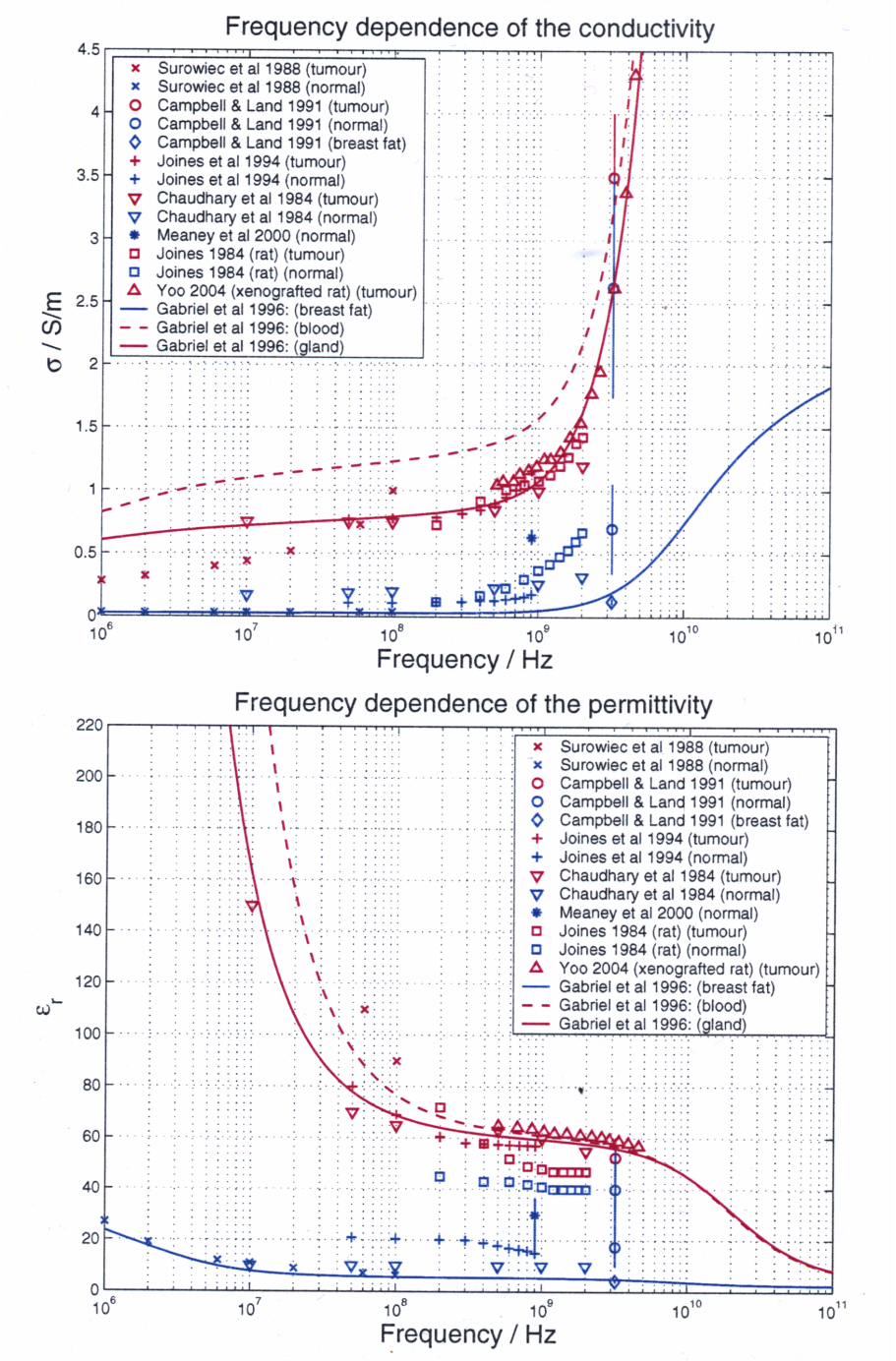

Figure 1.1: Literature values (Fhager, Gabriel et al, and others) of the conductivity and relative permittivity for normal (blue) and malignant (red) breast tissue

2 Model

2.1 Direct problem

To simulate wave propagation in media, well-known FDTD (Finite Difference in Time Domain) method is used (Taflove [25], Sadiku [26], Kunz and Luebbers [27]). It is based on a finite difference approximation of Maxwell equations.

2.1.1 Maxwell equations

Maxwell equations is a set of equations that describe the interrelationship between electric fields, magnetic fields, electric charge, and electric current. It consists of four Laws.

Faraday's Law of Induction:

$$\nabla \times \mathbf{E} = -\frac{\partial \mathbf{B}}{\partial t}$$

Ampere's Circuital Law:

$$\nabla \times \mathbf{H} = \mathbf{J} + \frac{\partial \mathbf{D}}{\partial t}$$

Gauss Law:

$$\nabla \cdot \mathbf{D} = \rho$$

Gauss Law for Magnetism (absence of magnetic monopoles):

$$\nabla \cdot \mathbf{B} = 0$$

Where:

E - electric field vector, $[V/m]$;

D - electric flux density vector, $[C/m^2]$;

H - magnetic field vector, $[A/m]$;

B - magnetic flux density vector, $[Wb/m^2]$;

J - electric conduction current density, $[A/m^2]$.

The following relation holds for linear, isotropic, non-dispersive material:

$$\mathbf{D} = \epsilon \mathbf{E}$$

$$\mathbf{B} = \mu \mathbf{H}$$

$$\mathbf{J} = \sigma \mathbf{E}$$

Where:

μ - magnetic permeability, $[H/m]$;

ϵ - electric permittivity, $[F/m]$;

σ - electric conductivity, $[S/m]$.

With these assumptions about the material the following representation of the Ampere's and Faraday's laws can be derived:

$$\frac{\partial \mathbf{E}}{\partial t} = \frac{1}{\epsilon} \nabla \times \mathbf{H} - \frac{\sigma}{\epsilon} \mathbf{E} \tag{2.1}$$

$$\frac{\partial \mathbf{H}}{\partial t} = -\frac{1}{\mu} \nabla \times \mathbf{E} \tag{2.2}$$

For each coordinate the Equation (2.1) can be written in terms of the x, y and z components:

$$\begin{cases} \frac{\partial E_x}{\partial t} = \frac{1}{\epsilon} \left(\frac{\partial H_z}{\partial y} - \frac{\partial H_y}{\partial z} - \sigma E_x \right) \\ \frac{\partial E_y}{\partial t} = \frac{1}{\epsilon} \left(\frac{\partial H_x}{\partial z} - \frac{\partial H_z}{\partial x} - \sigma E_y \right) \\ \frac{\partial E_z}{\partial t} = \frac{1}{\epsilon} \left(\frac{\partial H_y}{\partial x} - \frac{\partial H_x}{\partial y} - \sigma E_z \right) \end{cases} \tag{2.3}$$

Equation (2.2) can be written in the similar way.

This is a continuous differential equation. To solve them on a computer it is necessary to rewrite them in discrete form.

2.1.2 Discrete form of equations

The computing scheme for Maxwell's equations was introduced by Yee in 1966 [28]. In this scheme the electric and the magnetic vectors are both placed on the edges of a separate cubic lattice and interleaved with each other. This is illustrated on Figure 2.1 (a). The time stepping is implemented as a leapfrog scheme. In each time step one variable is calculated from its value in the previous time step and the value of the second variable in the current time step. This is illustrated on the figure 2.1 (b).

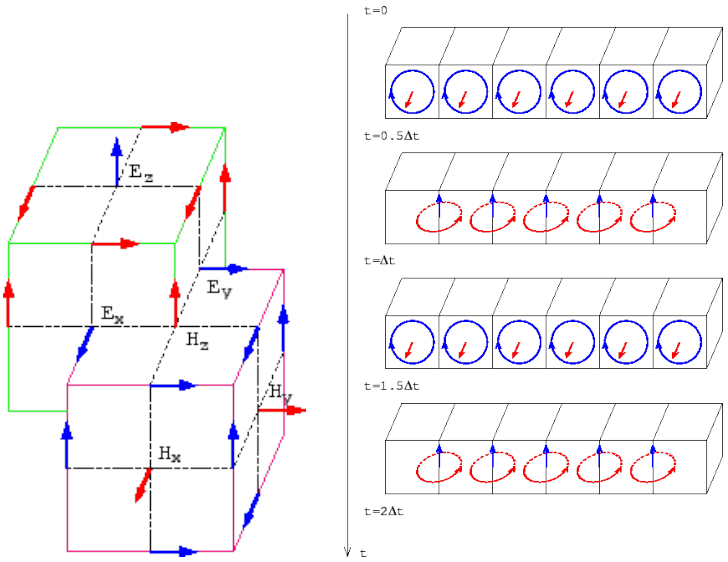

(a) Yee Cell (b) Leapfrog Scheme

Figure 2.1: Discrete Space and Time

Taking all this into consideration we can derive expression for the discrete equations. If i, j, k and n are integers, the field in a particular space-time point can be written as

$$u(i\Delta x, j\Delta y, k\Delta z, n\Delta t) = u|^n_{i,j,k}.$$

Here $\Delta x, \Delta y, \Delta z$ are spatial grid step sizes and Δt is a time step. As example, it is possible to write the first equation of 2.3 as

$$\frac{E_x|^{n+1}_{i,j,k} - E_x|^n_{i,j,k}}{\Delta t} = \frac{1}{\epsilon_{i,j,k}} \left(\frac{H_z|^{n+1/2}_{i,j+1/2,k} - H_z|^{n+1/2}_{i,j-1/2,k}}{\Delta y} - \frac{H_y|^{n+1/2}_{i,j,k+1/2} - H_y|^{n+1/2}_{i,j,k-1/2}}{\Delta z} - \sigma_{i,j,k} E_x|^{n+1/2}_{i,j,k} \right)$$

In FDTD a stability condition have to be used to ensure that the wave will not propagate through a cell with a speed higher than the speed of light. Taflove and Brodwin [29],

showed that to guarantee numerical stability the time step Δt should fulfill the condition

$$c\Delta t \leq \left(\frac{1}{(\Delta x)^2} + \frac{1}{(\Delta y)^2} + \frac{1}{(\Delta z)^2} \right)^{-1/2} \tag{2.4}$$

In case of a cubic lattice where $\Delta x = \Delta y = \Delta z = \Delta$ the condition reduces to

$$\Delta t = \frac{\Delta}{c\sqrt{3}} \tag{2.5}$$

where c is the speed of light.

2.1.3 Complex permittivity

The relative permittivity of a medium can be represented by a complex quantity ϵ'_r, that has a real ϵ_r part describing energy storage and imaginary part ϵ''_r describing energy losses. The value of the permittivity varies as a function of the frequency of the applied electromagnetic field:

$$\epsilon'_r(\omega) = \epsilon_r(\omega) - j\epsilon''_r(\omega)$$

Here $j^2 = -1$ and ω is the angular frequency ($\omega = 2\pi F$, where F is frequency expressed in Hertz). The imaginary part is the sum of a conductivity term and a relaxation term ([30]):

$$\epsilon''_r(\omega) = \frac{\sigma}{\omega\epsilon_0} + \epsilon''_{r,relaxation}(\omega)$$

where σ is ionic conductivity in Siemens per meter, $\epsilon_0 = 8.8542 \times 10^{-12} F/m$ is permittivity in vacuum and $\epsilon''_{r,relaxation}$ is the loss due to dielectric relaxation.

In our model relaxation is not implemented, thus the complex permittivity is

$$\epsilon'_r(\omega) = \epsilon_r - j\frac{\sigma}{\omega\epsilon_0} \tag{2.6}$$

Using this model either real (relative permittivity) or imaginary (conductivity) part of the complex permittivity could be better reconstructed depending on the frequency.

Model for complex permittivity was derived by Debye [31]:

$$\epsilon(\omega) = \epsilon_\infty + \frac{\Delta\epsilon}{1 + i\omega\tau}$$

where ϵ_∞ is the permittivity at the high frequency limit, $\Delta\epsilon = \epsilon_s - \epsilon_\infty$ where ϵ_s is the static, low frequency permittivity and τ is the characteristic relaxation time of the medium.

More accurate empirical function was suggested by Cole and Cole [32, 33]:

$$\epsilon(\omega) = \epsilon_\infty + \sum_n \frac{\Delta\epsilon_n}{1 + (i\omega\tau_n)^{(1-\alpha_n)}} + \frac{\sigma_s}{i\omega\epsilon_0}$$

where σ_s is static conductivity.

2.2 Inverse problem

The inverse problem is about finding the properties of the media based on some measurements. The inverse problem is the opposite of the direct problem, where the propagation through the media is computed based on the knowledge of the material properties. From a cause-effect point of view the direct problem can be seen as finding the effect from given cause. The inverse problem is instead to determine the cause from an observed effect (Tarantola [34], Bertero and Boccacci [35]).

2.2.1 Stability of inverse problems

In 1902 Hadamard formulated the conditions of a well-posed problem:

1. A Solution should exist for any data
2. The Solution should be unique
3. The Solution should be stable, or continuously depend on input data, i.e. small variations in the input data should correspond to the small variations in the output data (not large errors)

If any of these criteria are not fulfilled, the problem is referred to as an ill-posed problem.

The inverse electromagnetic problem is ill-posed due to the third criteria (Colton and Kress [36]; Isakov [37], Colton and Paivarinta [38]).

Whether a problem is ill-posed or well-posed is determined by the differential operator, data and solution space and their norms. To cure an ill-posed problem one could change the operator or the problem solution spaces. Usually this is not possible due to the physical nature of the problem, since the data space should, for example, be able to contain all the measurements. Another approach is to use regularization (Tikhonov [39]) which is based on the idea that approximate solution can be found with some additional a priori data is incorporated. It is also possible to use a Bayesian approach to solve inverse problems of tomography ([40, 41, 42]). In this work regularization approach is taken.

2.3 Minimization Functional

The imaging problem is formulated as a minimization of the functional

$$F(\epsilon,\sigma)=\sum_{m=1}^{M}\int_0^T\sum_{n=1}^{N}|\mathbf{E}_m^{sim}(\epsilon,\sigma,\mathbf{R}_n,t)-\mathbf{E}_m^{meas}(\mathbf{R}_n,t)|^2dt, \tag{2.7}$$

where $\mathbf{E}_m^{sim}(\epsilon,\sigma,\mathbf{R}_n,t)$ is the calculated field from the computational model of the setup, and $\mathbf{E}_m^{meas}(\mathbf{R}_n,t)$ is the measured data. M is the number of transmitters and N is the number of receivers. $\mathbf{R}_n$ is the position of the n-th receiver, T is the time of one the simulation.

The solution is obtained by minimization of this non-linear functional using optimization methods. The minimum will correspond to the best fit of the conductivity and permittivity to the measured data.

2.4 Nonlinear optimization methods

2.4.1 Steepest Descent

Steepest descent is a method for local minimum search [43]. It starts from point x^0 and, as many times as needed, moves from point $x^{(i)}$ to $x^{(i+1)}$ by minimizing in the direction of $-\nabla f(x^{(i)})$, the local downhill gradient. The new iteration is determined by

$$x^{(i+1)}=x^{(i)}-\delta^{(i)}\nabla f(x^{(i)}), \tag{2.8}$$

where the step size δ is determined from a linear search in the negative direction of the gradient.

2.4.2 Conjugate Gradient

If the target function is shaped as a long narrow valley with the miminum at the ottom of the valley, the steepest descent method will be very inefficient in stepping toward the minimum. Conjugate gradient method uses conjugate directions instead of the local gradient for going downhill ([44]). If the vicinity of the minimum has the shape of a long, narrow valley, the minimum is reached in far fewer steps than would be the case using the method of steepest descent. The update rule for the conjugate gradient is as follows:

$$x^{(i+1)}=x^{(i)}+\alpha_i d^{(i)} \tag{2.9}$$

where $d^{(i)}$ is conjugate direction and α_i is the step length that is determined from a linear minimum search in direction $d^{(i)}$. The direction could, for example, be determined by

using the Flethcer-Reeves equation:

$$d^{(i+1)} = r^{(i+1)} + \beta^{(i+1)} d^{(i)} \tag{2.10}$$

where

$$r^{(i)} = -\nabla f(x^{(i)}) \tag{2.11}$$

and

$$\beta^{(i+1)} = \frac{r^T_{(i+1)} r_{(i+1)}}{r^T_{(i)} r_{(i)}} \tag{2.12}$$

Equation (2.10) means that new conjugate direction is the sum of antigradient at the current point and the previous direction multiplied by the coefficient (2.12). Fletcher and Reeves suggests to restart algorithmic procedure every $n + 1$ steps, where n is the search space dimension. Another method of computing $\beta^{(i+1)}$ was suggested by Polak and Ribbiere:

$$\beta^{(i+1)} = \frac{r^T_{(i+1)} (r_{(i+1)} - r_{(i)})}{r^T_{(i)} r_{(i)}} \tag{2.13}$$

The Fletcher-Reeves method converges if starting point is close enough to the minimum, while the Polak-Ribiere method sometime can cycle forever. However the latter often converges faster then the first. Convergence of Polak-Ribiere method can be guaranteed by choosing $\beta = max\{\beta, 0\}$. This is equivalent to the restart of algorithm if $\beta \leq 0$. Restart of the algorithmic procedure is necessary to "forget" the last direction and start algorithm again in the direction opposite to the gradient.

2.4.3 Newtons method

In contrast to the steepest descent and the conjugate gradient methods, which are first-order methods, Newtons method is a second-order minimization method. If a real number x^* is a stationary point (minima or maxima) of the function $f(x)$, then x^* is a root of the derivative $f\prime(x)$. Consider Taylor's expansion:

$$f(x + \delta x) = f(x) + f\prime(x)\delta x + \frac{1}{2} f\prime\prime(x)\delta x^2 + ... \tag{2.14}$$

Function $f(x)$ is minimized when δx solves the equation

$$f\prime(x) + f\prime\prime(x)\delta x = 0 \tag{2.15}$$

and $f\prime\prime(x)$ is positive. Thus provided that $f(x)$ is twice-differentiable function and the initial guess x_0 is chosen close enough to the x^*, the sequence (x_n) defined by

$$x_{n+1} = x_n - \frac{f\prime(x_n)}{f\prime\prime(x_n)}, \; n > 0 \tag{2.16}$$

will converge toward x^*.

This iterative scheme can be generalized to several dimensions by replacing the derivative with the gradient $\nabla f(x)$, and the reciprocal of the second derivative with the inverse of the Hessian matrix $H_f(x)$:

$$H_f(x) = \begin{bmatrix} \frac{\partial^2 f}{\partial x_1^2} & \frac{\partial^2 f}{\partial x_1 \partial x_2} & \cdots & \frac{\partial^2 f}{\partial x_1 \partial x_n} \\ \frac{\partial^2 f}{\partial x_2 \partial x_1} & \frac{\partial^2 f}{\partial x_2^2} & \cdots & \frac{\partial^2 f}{\partial x_2 \partial x_n} \\ \vdots & \vdots & \ddots & \vdots \\ \frac{\partial^2 f}{\partial x_n \partial x_1} & \frac{\partial^2 f}{\partial x_n \partial x_2} & \cdots & \frac{\partial^2 f}{\partial x_n^2} \end{bmatrix} \tag{2.17}$$

Then the update rule is

$$x^{(i+1)} = x^{(i)} - \frac{1}{H_f(x^{(i)})} \nabla f(x^{(i)}). \tag{2.18}$$

This method requires second derivatives of the target function, which is expensive to compute in this application, since requires $2n^2$ evaluations of target function to compute Hessian numerically. Analytical expression for Hessian could resolve this complexity.

2.4.4 Gauss-Newton method

This method is used to solve the nonlinear least squares problems. It is a modification of Newton's method that does not use second derivatives. This method works when the target function $f(x)$ is sum of squares of functions $g_i(x)$.

$$f(x) = ||g(x)||^2 \tag{2.19}$$

In this case of sum of squares the Hessian is replaced by multiplication of two Jacobians:

$$x^{(i+1)} = x^{(i)} - \frac{1}{J_g(x^{(i)})^T J_g(x^{(i)})} J_g(x^{(i)})^T g(x^{(i)}) \tag{2.20}$$

or

$$(J_g(x^{(i)})^T J_g(x^{(i)}))(\Delta x)^{(i)} = -J_g(x^{(i)})^T g(x^{(i)}) \tag{2.21}$$

In our application it is not possible to analytically find an expression for the Jacobian $J_g(x)$ of the single component of the sum in Equation (2.7), which is necessary to find Hessian. Analitical gradients we use are based on the sum in Equation (2.7), not on a single component of the sum. That is why it is only possible to find expression for

Jacobian of the sum $J_{||g||^2}(x)$, which is not enough to represent Hessian $H_f(x)$. This is the reason why this method is not applicable for our reconstructions.

2.4.5 Levenberg-Marquardt

This method is a combination of Steepest Descent and Gauss-Newton method. The algorithm was first published by Kenneth Levenberg [45], while working at the Frankford Army Arsenal. It was rediscovered by Donald Marquardt [46] who worked as a statistician at DuPont.

The update rule in this case is:

$$(J_g(x^{(i)})^T J_g(x^{(i)}) + \lambda I)(\Delta x)^{(i)} = -J_g(x^{(i)})^T g(x^{(i)}) \tag{2.22}$$

Since we can not use Gauss-Newton method for our reconstruction for the reason explained in the previous section, Levenberg-Marquardt method also can not be used.

2.4.6 Quasi-Newton Methods

Quasi-Newton methods are based on Newton's method, but they approximate the Hessian matrix, or its inverse, in order to reduce the amount of computation per iteration.

The most widespread is BFGS method that was suggested independently by Broyden, Fletcher, Goldfarb, and Shanno, in 1970.

The principal idea of the method is to construct an approximate Hessian matrix of the second derivatives of the function to be minimized, by analyzing successive gradient vectors. The Hessian matrix does not need to be computed at any stage. However, the method assumes that the function can be locally approximated as a quadratic function in the region around the optimum.

The update formula for the approximate Hessian is

$$H_{k+1} = H_k + \frac{q_k q_k^T}{q_k^T s_k} - \frac{H_k^T s_k^T s_k H_k}{s_k^T H_k s_k} \tag{2.23}$$

where

$$s_k = x_{k+1} - x_k$$
$$q_k = \nabla f(x_{k+1}) - \nabla f(x_k)$$

As a starting point, H_0 can be set to any symmetric positive definite matrix, for example, the identity matrix I. To avoid the inversion of the Hessian H, it is possible to derive an updating method that avoids the direct inversion of H by using a formula that makes an approximation of the inverse Hessian at each update.

At each major iteration, k, a line search is performed in the direction similar to the (2.18)

$$d = -H_k^{-1} \cdot \nabla f(x_k)$$

L-BFGS is a limited-memory quasi-Newton method (Nocedal [47]). L-BFGS stands for "Limited memory BFGS method"; instead of storing a full approximation to the Hessian, a low rank approximation is updated.

2.5 Regularization

In order to make the ill-posed reconstruction problem well-posed regularization is used.

2.5.1 Tikhonov regularization

Tikhonov regularization [39] is the most commonly used method for regularization of ill-posed problems. In some fields, it is also known as ridge regression.

In its simplest form, an ill-conditioned system of linear equations

$$A\mathbf{x} = \mathbf{b}, \tag{2.24}$$

where A is an $m \times n$ matrix above, $\mathbf{x}$ is a column vector with n entries and $\mathbf{b}$ is a column vector with m entries, is replaced by the problem of seeking an $\mathbf{x}$ to minimize

$$\|A\mathbf{x} - \mathbf{b}\|^2 + \alpha^2\|\mathbf{x}\|^2 \tag{2.25}$$

for some suitably chosen Tikhonov factor $\alpha > 0$. Here $\|\cdot\|$ is the Euclidean norm. This improves the conditioning of the problem, thus enabling a numerical solution. An explicit solution, denoted by $\hat{\mathbf{x}}$, is given by:

$$\hat{\mathbf{x}} = (A^T A + \alpha^2 I)^{-1} A^T \mathbf{b} \tag{2.26}$$

where I is the $n \times n$ identity matrix. For $\alpha = 0$ this reduces to the least squares solution provided that $(A^T A)^{-1}$ exists.

The following analogy can be made: for tomography problem $\mathbf{x}$ is the conductivity and the permittivity distribution that we are reconstructing, A is linear approximation of the FDTD method, $\mathbf{b}$ is the measurements vector.

2.5.2 Generalized Tikhonov regularization

For $\mathbf{x}$ and the data error, one can apply a transformation of the variables to reduce to the case above. Equivalently, one can seek an $\mathbf{x}$ to minimize

$$\|A\mathbf{x} - \mathbf{b}\|_P^2 + \alpha^2\|\mathbf{x} - \mathbf{x}_0\|_Q^2 \tag{2.27}$$

where we have used $\|\mathbf{x}\|_P$ to represent for the weighted norm $\mathbf{x}^T P\mathbf{x}$.

This can be solved explicitly using the formula

$$\mathbf{x}_0 + (A^T PA + \alpha^2 Q)^{-1} A^T P(\mathbf{b} - A\mathbf{x}_0).$$

See Ulbrich [48] for more details.

2.5.3 Total Variation regularization

Edge-preserving properties of a total variation regularization described by Strong and Chan [49]. The regularization term added to the original functional in this case is

$$R_{TV}[f] = \int |\nabla f(\mathbf{x})| d\mathbf{x}. \tag{2.28}$$

This approach serves quite well for noise removal problems and restoring images with larger-scaled features.

2.5.4 Variance uniformization

Cohen-Bacrie et. al. [50] suggests that the amount of regularization should vary spatially. It was found that the information is richer in peripheral region than in central region, since transmitters and receivers are not in the center. Since the Tikhonov approach applies a constant amount of regularization over the domain, they proposed a modification such that the regularization level varied spatially. Instead of the Tikhonov regularization term $\lambda x^T x$ they derived a new regularization matrix R for the term $x^T Rx$, where R is a positive semidefinite matrix. R was derived to fulfill variance uniformization constraint: more regularization applied to the central regions then to the peripheral regions. Two regularization parameters were introduced to determine R. One was the truncation degree of singular value decomposition and another was the level of variance. Both of these parameters were determined automatically by ordinary and generalized cross-validations from measured data only.

Presented results shows that the method performs better than Tikhonov regularization for Electrical Impedance Tomography.

2.5.5 Nonlinear regularization

This type of regularization is described by Roths et. al. [51]. Tikhonov regularization can be represented as

$$R^{TIK}[f] = \int_{I_S} (Lf(s))^2 ds, \tag{2.29}$$

where L is linear operator. L is usually chosen as identity (f limited) or second derivative (f smooth), i.e. $L = 1$ or $L = \partial_s^2$. They propose to replace this regularization term with the less restrictive

$$R[f] = \int_{I_S} ds(O[f](s))^2, \tag{2.30}$$

with O now being more general, in particular nonlinear operator whose variational derivative $\delta O/\delta f$ with respect to f exists.

As example they propose edge-preserving (EPR) regularization represented as the term

$$R_\alpha^{EPR}[f] = \int_{I_S} ds \frac{(f''(s))^2}{\sqrt{1 + (\alpha f''(s))^2}}. \tag{2.31}$$

A self consistent method is used to determine the regularization parameter. This type of regularization is implemented as publicly available library [51].

2.5.6 Edge-Preserving regularization

Edge-Preserving regularization has been used in many papers (Casanova et. al. [52], Yoshida et. al. [53], Lobel et. al.[54, 55, 56], Charbonnier et. al. [57, 58, 59]). This type of regularization has been chosen for more detailed study since it has a strong theoretical foundation with more flexibility than other methods, and numerous applications tested that it works [52, 53], as well as some algorithms (e.g. half-quadratic regularization) for efficient solving of minimization problem. Regularization is added by replacement of the original functional with a new one:

$$F_1(\epsilon, \sigma) = F(\epsilon, \sigma) + F_R(\epsilon, \sigma). \tag{2.32}$$

The regularization term is defined as

$$F_R(\epsilon, \sigma) = F_{R\epsilon}(\epsilon) + F_{R\sigma}(\sigma), \tag{2.33}$$

$$F_{R\epsilon}(\epsilon) = \lambda_\epsilon \int_\Omega \varphi(\nabla\epsilon) dS,$$

$$F_{R\sigma}(\sigma) = \lambda_\sigma \int_\Omega \varphi(\nabla\sigma) dS.$$

Here $\varphi(t)$ is regularizing function with the following requirements [56]: the homogeneous areas with the same permittivity are isotropically smoothed, while edges are preserved (i.e. smoothing of an edge is performed only in its tangential direction). Standard Tikhonov regularization ($\varphi(t) = t^2$) and total variations regularization ($\varphi(t) = t$) do not satisfy this condition. We can also see this regularization as a kind of generalization of other regularization methods with the possibility to imitate them.

To be able to find the minimum of the modified functional in equation (2.32) with gradient-based methods (e.g. steepest descent or conjugate gradient method) we would like to have an analytical expression of its gradient. We already have analytical solution for the original problem (Gustafsson [60]), so we have to derive only expression for the regularization term. Following Yoshida et. al. [53], we can find the new gradients by means of a Fréchet differentiation. Let us consider an infinitesimal variation $\delta\epsilon$ of the permittivity. Then we obtain

$$F_{R\epsilon}(\epsilon + \delta\epsilon) - F_{R\epsilon}(\epsilon) = \delta F_{R\epsilon}, \tag{2.34}$$

$$F_{R\epsilon}(\epsilon + \delta\epsilon) - F_{R\epsilon}(\epsilon) = \lambda_\epsilon \int_\Omega \varphi(\nabla\epsilon + \nabla\delta\epsilon) - \varphi(\nabla\epsilon) dS. \tag{2.35}$$

From

$$\varphi(\nabla(\epsilon + \delta\epsilon)) - \varphi(\nabla\epsilon) = \varphi\prime(\nabla\epsilon)\nabla(\delta\epsilon) + o(\delta\epsilon)$$

it is found that

$$\delta F_{R\epsilon}\delta\epsilon = \lambda_\epsilon \int_\Omega \varphi\prime(\nabla\epsilon)\nabla(\delta\epsilon) dS. \tag{2.36}$$

The right-hand side of equation (2.36) is integrated by parts

$$\int_\Omega \varphi\prime(\nabla\epsilon)\nabla(\delta\epsilon) dS = \int_\Gamma \varphi\prime(\nabla\epsilon)\delta\epsilon dl - \int_\Omega \nabla\varphi\prime(\nabla\epsilon)\delta\epsilon dS. \tag{2.37}$$

Considering $\delta\epsilon = 0$ on the boundary Γ of area Ω, variation $\delta F_{R\epsilon}$ will be

$$\delta F_{R\epsilon} = -\lambda_\epsilon \int_\Omega \nabla\varphi\prime(\nabla\epsilon)\delta\epsilon dS =< g_{R\epsilon}, \delta\epsilon >, \tag{2.38}$$

where the inner product $<,>$ is defined as

$$< a(x), b(x) >= \int\int_S a(x)b(x) dS \tag{2.39}$$

Then after an analog calculation for the conductivity variable

$$\begin{aligned} \delta F_R(\epsilon, \sigma) &=< g_{R\epsilon}, \delta\epsilon > + < g_{R\sigma}, \delta\sigma >, \\ g_{R\epsilon} &= -\lambda_\epsilon \nabla\varphi\prime(\nabla\epsilon), \\ g_{R\sigma} &= -\lambda_\sigma \nabla\varphi\prime(\nabla\sigma). \end{aligned} \tag{2.40}$$

This is the only change that should be introduced to original algorithm to replace Tikhonov regularization with edge-preserving regularization. To get back original Tikhonov regularization term we can take $\varphi(t) = t^2$ with $\varphi\prime(t) = 2t$ to get

$$g_{R\epsilon} = -\lambda_\epsilon \nabla(2\nabla\epsilon) = -2\lambda_\epsilon \nabla^2\epsilon, \tag{2.41}$$

which is exactly the term presented in [16].

The next important step is to chose a function φ. By Charbonnier et. al. [59] properties of such a function were presented. Table 2.1 contains examples of such functions, which are also shown in the Figure 2.2.

	Ref.	$\varphi(t)$	$\varphi\prime(t)$
φ_{GM}	[61]	$\frac{t^2}{1+t^2}$	$\frac{2t}{(1+t^2)^2}$
φ_{HL}	[62]	$log(1+t^2)$	$\frac{2t}{1+t^2}$
φ_{HS}	[58]	$2\sqrt{1+t^2}-2$	$\frac{2t}{\sqrt{1+t^2}}$
Tikhonov Reg.		t^2	$2t$

Table 2.1: Edge-preserving potential functions

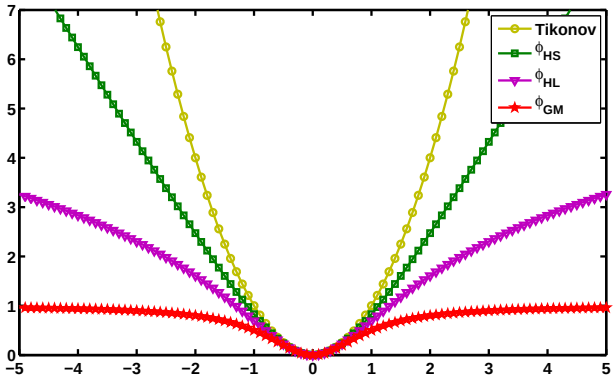

Figure 2.2: Potential functions

For this report φ_{GM} was chosen for comparison to Tikhonov regularization. It is possible to pick other functions, or the modified for better fine-tuning (Yoshida et. al. [53]) function like:

$$\varphi(t) = \varphi(t,\xi) = \frac{(t/\xi)^2}{1+(t/\xi)^2},$$

with scaling parameter ξ and derivative

$$\varphi\prime(t,\xi) = \frac{2t/\xi^2}{(1+(t/\xi)^2)^2}.$$

However this brings one extra parameter ξ to determine, thus it is not a good solution from computational point of view since without automated procedure for the parameter determination it is done by time consuming test reconstructions for each parameter value.

2.5.7 New specialized regularization

The type of regularization described in the following can be seen as one possible specialization of a generalized regularization specifically for reconstruction of the tumor in the healthy tissue. But as a start let's look at the edge-preserving regularization again. During the studies in this work the potential function $\varphi_{GM}(t) = \frac{t^2}{1+t^2}$ was used. But what is dimension of this function? And how much penalization should be applied to the original function? This questions should be answered in order to use the regularization. Looking for regularization parameter in range from minus infinity to plus infinity is not a good choice. Let us recall our new regularized minimization functional:

$$F(\epsilon,\sigma) = \int_0^T \sum_{m=}^{M}\sum_{n=1}^{N}(|\mathbf{E}_m(\epsilon,\sigma,\mathbf{R}_n,t) - \mathbf{E}_m^{meas}(\mathbf{R}_n,t)|^2)dt + \\ + \lambda_\epsilon \int_\Omega \varphi(\nabla\epsilon)dS + \lambda_\sigma \int_\Omega \varphi(\nabla\sigma)dS$$

In this functional electric field vector $\mathbf{E}$ is measured in volts per meter, and it should be related by the coefficients λ and the potential function $\varphi(t)$ to the spatial derivatives $\nabla\epsilon$ of the permittivity and $\nabla\sigma$ of the conductivity: permittivity ϵ measured in Farads per meter, and electric conductivity σ measured in Siemens per meter. With the different dimensions of the different terms we should find how much regularization should be applied for the optimal performance. If we apply too much, then the minimization will work only to minimize the regularization term, but will not ensure that simulated solution is in accordance with the measurements. On the other hand, if the regularization terms are too small, then noise will affect the solution too much, since some values that are not a correct solution will give a field pattern after simulation with a good agreement with the measurements. To prevent it we should penalize high "jumps" in the solution.

Another consideration is that we want to recognize objects that are very different from the background properties. We want to preserve this transition from the background to the object in one or two grid cell steps, but we want to penalize small noise variations inside the object and in the background area. Furthermore, we also want to penalize very big peaks that appear due to the fact that the problem is ill-posed. This could, for example, be done by introduction of a cubically shaped function (see Figure 2.3). There should be no penalization for non-existing gradients ($\varphi(0) = 0$). Then penalization function should increase with first peak corresponding to small noise we want to suppress. Then penalization function should decrease with a minimum that corresponds to the

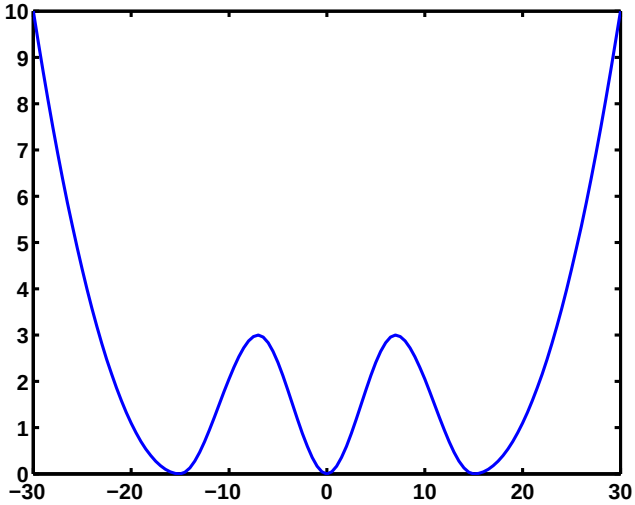

Figure 2.3: Symmetrical Potential function with a minimum

expected transition from the background to the object. Gradients that are bigger than the expected contrast should be penalized. Here arises another parameter to determine: how much should we penalize the small noise?

If we will take our potential function as polynomial, then we can summarize conditions as following:

$$\begin{cases} \varphi(0) = 0 \\ \varphi'(t_{expected\,contrast}) = 0\ (min) \\ \varphi'(t_{small\,noise}) = 0\ (max) \end{cases}$$

Potential function should be symmetric, so we should use polynomial function of higher order to achieve that, or just take absolute value of t before applying function to it. This type of potential function was not investigated in this thesis, but only the suggestion is that it could work. It can be investigated later, especially having some procedure for automated determination of multiple regularization parameters.

2.5.8 Regularization parameter

Let us say we want 50% of minimization functional to be determined by original misfit functional and other 50% by regularization terms. The misfit functional consists of $N * M * T$ residuals between simulated and measured electric field in V/m, where M is

number of transmitters, N is number of receivers and T is number of discrete time steps of one simulation were taken. We should relate it to the potential function of spatial derivative values under investigation. The derivatives are measured in F/m per grid step and S/m per grid step. Determination of this regularization parameter is a fairly difficult problem and the usual solution is to try several different parameters to see which works better. The considerations above gives only rough ideas of what to expect to work well.

There are automated methods to determine regularization parameter, e.g. the cross-validation technique (Wahba et. al. [63], [64], Hansen [65]). Generalized Cross-Validation is based on the philosophy that if an arbitrary measurement on the receiver is left out, then the corresponding regularized solution should predict this observation well. Detailed study of this technique is outside of the scope of this work.

3 Simulations

During the simulations the main point was to investigate how Tikhonov and Edge-Preserving regularizations help to reconstruct the object in the presence of noise in the measurements. For the simulations a simple object that is located in the center of the reconstruction domain was chosen (Figure 3.1). Then a frequency content of the illumination pulse was found to resolve the object well. This frequency depends on the size of the object and on the permittivity of the background where the wave propagates. Different amounts of noise were added to the signal to investigate how algorithm will reconstruct the noisy data for different values of the regularization parameters λ_ϵ and λ_σ.

3.1 Simulation setup

For the simulation special parameters have to be carefully chosen. Most of them are related and dependent on each other. For example the time step for the FDTD simulation is dependent on the spatial grid size. The duration of the simulation is dependent on the physical size of the simulation area and on the frequency width of the emitted pulse. The pulse width depends on the central frequency, which in turn should be chosen in relation to the object size and permittivity of the background material.

The physical size of the simulation domain is determined by the experimental setup. The setup used is a uniform background with a small object in the middle. Transmitter-receiver antennas are evenly distributed around the object on a circle. Simulation area should be bigger than the antennas. The simulations are conducted in an open space, corresponding to an infinite simulation domain. To model this infinity, absorbing boundary conditions (Mur [66]) are used.

The domain is covered by a finite grid. The number of points on the grid is determined by the required accuracy and computational time: the finer the grid (smaller cells) the more accurate the simulation and the more time the simulation will require. More cells for the inverse problem will give extra variables to reconstruct and will make the inverse problem more unstable. Regularization will make solution stable and will give possibility to use a finer grid, but still will cause extra computational efforts.

Knowing the grid step, we can determine the time step using equation (2.5).

To determine the simulation time it is necessary to consider the time required for the wave to be emitted, then travel to the most distant edge and then reach the most distant

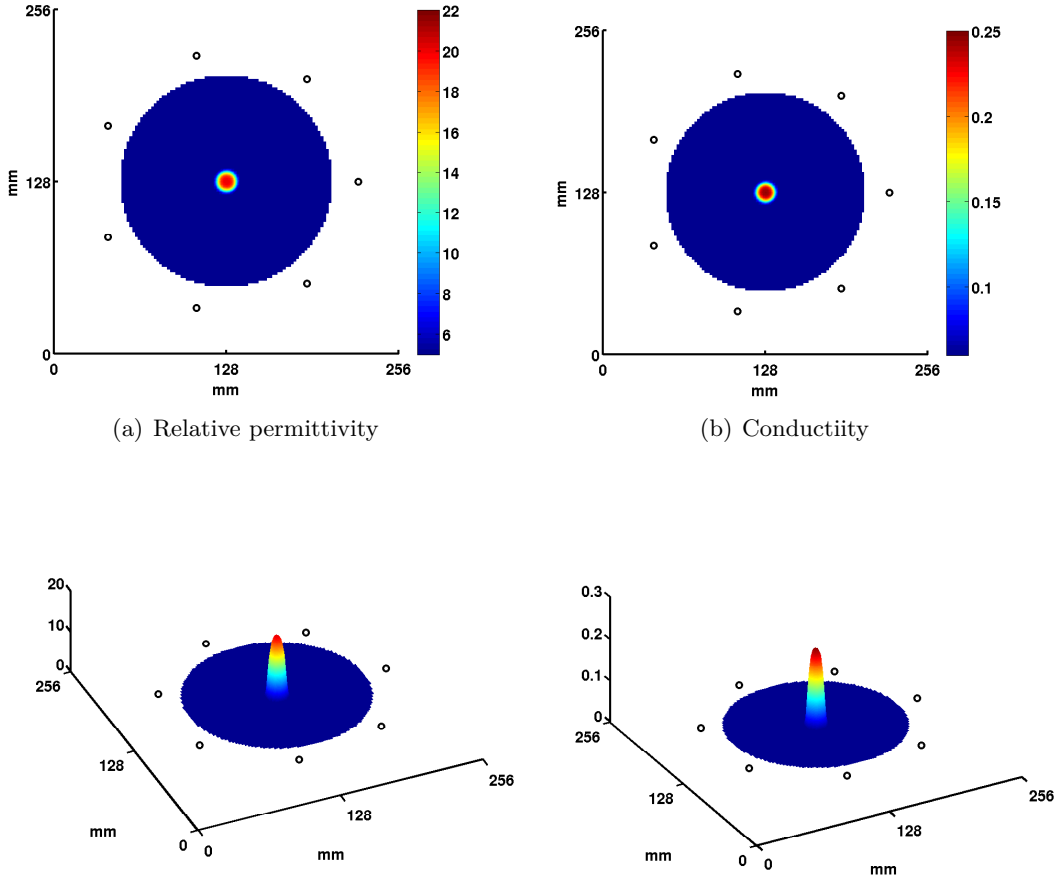

(a) Relative permittivity

(b) Conductiity

(c) Relative permittivity

(d) Conductivity

Figure 3.1: Object for simulations

receiver. The duration of the pulse emission depends on the frequency width of the pulse, see Figure 3.2.

Fhager et. al. [67] showed that the wider frequency width benefits reconstruction. The frequency width is limited by the central frequency: the width can not be more than central frequency, otherwise the width of the pulse will spread to negative frequency, which is not possible (see Figure 3.2). Based on the experience, the central frequency and corresponding wavelength should be in accordance with the size of the object we want to image:

$$\lambda = \frac{c}{\sqrt{\epsilon_r} f}.$$

where λ is the wavelength in the media, $c = 299792458$ m/s is the speed of light and f is the frequency in Hz. For the frequency 3 GHz and background relative permittivity

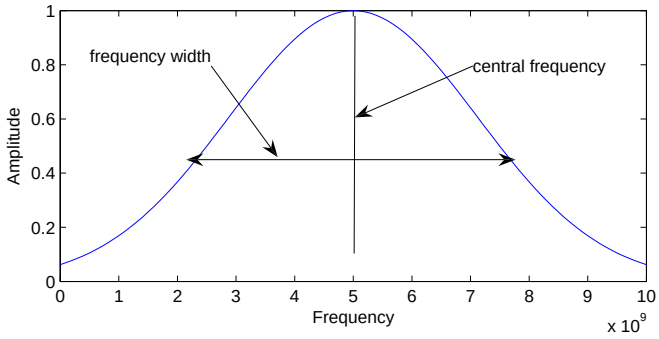

Figure 3.2: Gauss pulse in the frequency domain

5 that was used during the simulations, we will get wavelength $\lambda \sim 44$ mm, and this is roughly the size of the object that can be imaged. If the frequency is too high, the reconstruction will be too noisy and unstable, and if the frequency is too low, the reconstruction will be oversmoothed. The best approach for imaging objects with different sizes would be to use different frequencies, lower frequency components to reconstruct general features, and then higher to reconstruct finer features.

Another frequency issue is connected with the complex permittivity, equation (2.6). When the frequency is increasing, the imaginary part of the complex permittivity will be very small compared to the real part. In this case it will not be possible to reconstruct the conductivity. On the other hand, if frequency is too low, then we will be able to reconstruct only conductivity but not permittivity. Since we are using pulse with a range of frequencies, central frequency should be related to conductivity and permittivity of the media under investigation. Depending on media properties booth real and imaginary part of (2.6) should be of the same order.

As already mentioned, central frequency should be chosen in relation to the size of the object, its conductivity and its permittivity. In practice it could be impossible to implement, for example when the size of the object requires higher frequency and its permittivity and conductivity requires lower frequency to reconstruct conductivity.

Taking all this into consideration, values used in the simulation in this work are summarized in the Table 3.1.

3.1.1 Regularization parameter

It is possible to make an attempt for an estimation of the regularization parameters. In this work background values $\epsilon_{bg} = 5$ for the relative permittivity and $\sigma_{bg} = 0.06$ S/m for the conductivity were used. Object had $\epsilon_{obj} = 20$ and $\sigma_{obj} = 0.24$ S/m. Then spatial derivative on the edge of the object will be $\nabla\epsilon = \frac{20-5}{\Delta}$, where Δ is spatial space of

Variable	Value
Domain size	~20 cm
Grid size	2 mm
Number of grid cells in the computational domain	128 x 128 cells
Simulation time	12 ns
Central Frequency	3 GHz
Frequency width	3 GHz
Object shape	$f(x,y) = \cos^2(\frac{(x_c-x)^2+(y_c-y)^2}{r^2})$ (the first peak)
Object position (x_c, y_c)	cell (64,64)
Object size (radius) r	4 grid cells = 8 mm
Absorbing layer width	8 grid cells = 16 mm

Table 3.1: Values for simulations

transition (if there is a smooth transition between the background and the object). Let us take that edge of object is smoothed and occupies $\Delta = 4mm$, then keeping in mind our grid cell size $\Delta x = 2mm$ (see Table 3.1) we will expect our gradient to be $\nabla\epsilon = 7$ per one grid step. Similar for conductivity we can expect for object $\nabla\sigma = 0.09$ S/m per grid step. All gradients smaller and greater than that we should suppress and penalize.

3.2 Error measures

To compare the results from the different simulations with the original object different approaches can be taken. It is possible to use the relative error for the permittivity as

$$\zeta_\epsilon = \sqrt{\frac{\sum_{i,j=1}^{K}(\epsilon_{i,j}^{reconstructed} - \epsilon_{i,j}^{original})^2}{\sum_{i,j=1}^{K}(\epsilon_{i,j}^{original} - \epsilon_{i,j}^{background})^2}} \tag{3.1}$$

The similar measures can be written for the conductivity.

It is possible to specialize this error measure and look preciesly if the values in this error measure are due to the errors in the object or due to the artifacts.

Relative error for the object can be defined as

$$\zeta_\epsilon^{object} = \sqrt{\frac{\sum_{i,j\in S_{obj}}(\epsilon_{i,j}^{reconstructed} - \epsilon_{i,j}^{original})^2}{\sum_{i,j\in S_{obj}}(\epsilon_{i,j}^{original} - \epsilon^{background})^2}}, \tag{3.2}$$

where S_{obj} is area containing the object. For the artifacts estimation $\zeta_\epsilon^{artifacts}$ the artifacts area $S_{artifacts} = S \backslash S_{obj}$ is used, where S is the total area for the error estimation

and $K_{artifacts}$ is a total number of grid cells in the $S_{artifacts}$:

$$\zeta_{\epsilon}^{artifacts} = \sqrt{\frac{\sum_{i,j \in S_{noise}} (\epsilon_{i,j}^{reconstructed} - \epsilon_{i,j}^{original})^2}{K_{artifacts}}}. \tag{3.3}$$

The third estimation (the contrast) can be defined as

$$\zeta_{\epsilon}^{contrast} = \frac{\max_{i,j \in S_{obj}} (\epsilon_{i,j}^{reconstructed}) - \max_{i,j \in S_{noise}} (\epsilon_{i,j}^{reconstructed})}{\max_{i,j \in S_{obj}} (\epsilon_{i,j}^{original}) - \max_{i,j \in S_{noise}} (\epsilon_{i,j}^{original})}. \tag{3.4}$$

The contrast shows any value of the object that is bigger than any artifact around the object. In such case the contrast is positive. If there is an artifact with value bigger, than all reconstructed values of the object, then contrast is negative. Negative contast will indicate if reconstruction gives object in the area, which originally does not contain the object.

Relative maximal error can be used to indicate how bad is the worst point of the reconstructed image and is defined as

$$\zeta_{\epsilon}^{maxerr} = \frac{max_{i,j \in S} (\epsilon_{i,j}^{reconstr} - \epsilon_{i,j}^{original})}{max_{i,j \in S} \epsilon_{i,j}^{original} - min_{i,j \in S} \epsilon_{i,j}^{original}} \tag{3.5}$$

Another error measure can be defined through finding the original object for the reconstructed data. Original object is represented by the function

$$g[x_c, y_c, r, h](x, y) = h \cdot \cos^2\left(\frac{(x - x_c)^2 + (y - y_c)^2}{r^2}\right) \tag{3.6}$$

where x_c and y_c are the coordinates of the center of the object, r is the radius of the object, h is the maximum value of the object (maximum conductivity or maximum relative permittivity), see Table 3.1. The values of x_c, y_c, r, h for the conductivity and permittivity are obtained from a minimization of the following functions:

$$F_{\sigma fit}(x_c, y_c, r, h) = \sum_{x,y} \left(\sigma_{x,y} - g[x_c, y_c, r, h](x, y)\right)^2 \tag{3.7}$$

$$F_{\epsilon fit}(x_c, y_c, r, h) = \sum_{x,y} \left(\epsilon_{x,y} - g[x_c, y_c, r, h](x, y)\right)^2 \tag{3.8}$$

For both permittivity and conductivity, the values of the object parameters can be found as arguments that deliver minimum to the functions (3.7) and (3.8):

$$\{x_x^{fit}, y_c^{fit}, r_{fit}, h_{fit}\} = \arg \min_{x_c, y_c, r, h} F_{fit}(x_c, y_c, r, h) \tag{3.9}$$

Original object, reconstructed values and fitted object are shown on Figure 3.3.

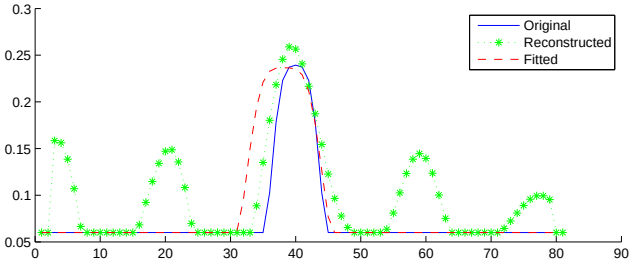

Figure 3.3: Original object, reconstructed values and fitted object

The "Radius" error measure can be defined as

$$\zeta_{rad} = r_{fit} \tag{3.10}$$

Maxima value of fitted object forms another error measure:

$$\zeta_{foreground} = h_{fit} \tag{3.11}$$

In this case we can determine where the object is located. A relative displacement error measure can be defined as

$$\zeta_{displacement} = \frac{\sqrt{(x_c^{fitted} - x_c^{orig})^2 + (y_c^{fitted} - y_c^{orig})^2}}{r_{orig}}. \tag{3.12}$$

The radius of the fitted object is a good estimation of how much the solution has been smoothed. Edge-preserving regularization should keep the radius as close as possible to the original, while Tikhonov regularization will introduce smoothness which will result in a bigger radius.

3.3 Simulation results

Simulations were conducted to check if the reconstructions are robust against the noise, and how the regularization can help archiving stability of the solution in the presence of noise. Tikhonov and Edge-preserving regularizations are compared.

As shown in the results, for chosen frequencies, object and background values, reconstruction of the permittivity is better then the reconstruction of the conductivity due to relation between the frequency and the complex permittivity described in Section 2.1.3.

3.3.1 Iterative reconstruction

To illustrate how reconstruction is improved from one iteration to another here is a plot of a typical example. The minimization functional decreases fast in the beginning, reaching some stable state after sufficient amount of iterations, and then only small refinements of the solution occurs. This is illustrated in the Figure 3.4. To make the visualization easier, crossections are given.

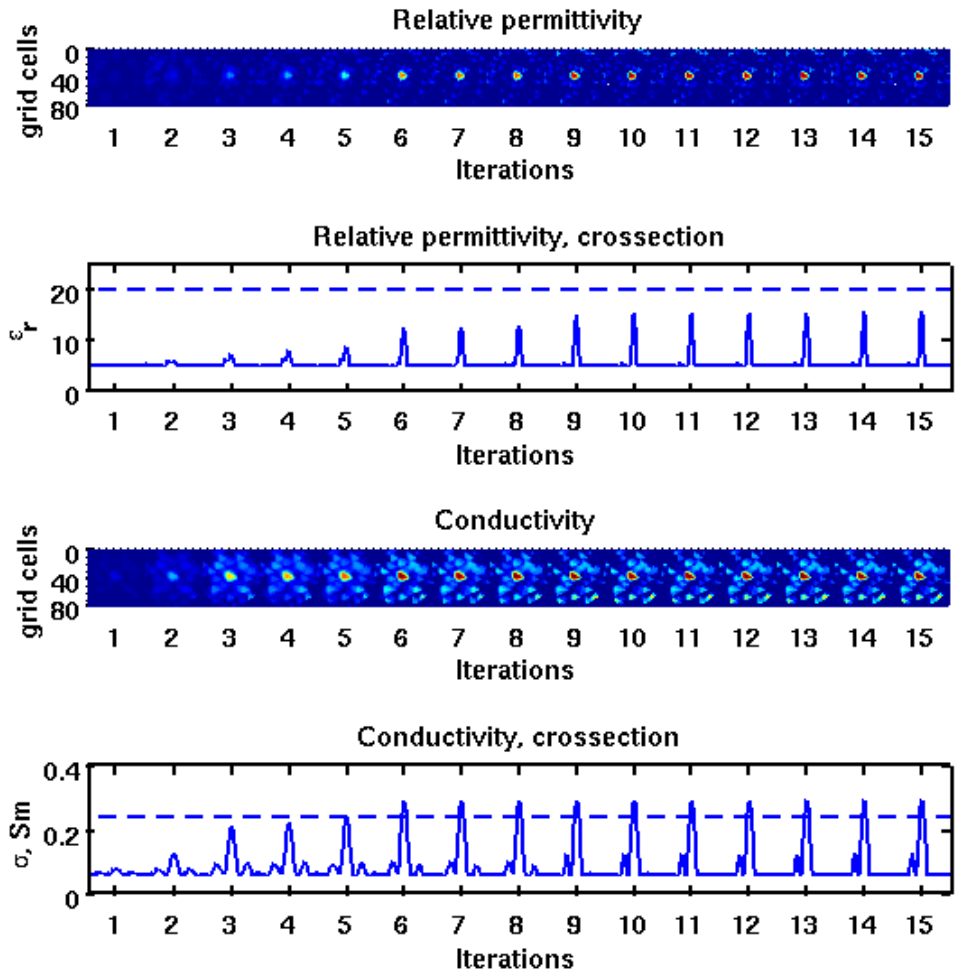

Figure 3.4: Example reconstruction

3.3.2 Sample reconstructions with and without noise

Since measured data always contain more or less noise, it is necessary to be able to work with noise also in the simulations. For the simulated data noise was added with Signal to Noise Ration (SNR) defined as

$$SNR = \frac{\int_0^T E^2 dt}{\int_0^T N^2 dt}$$

Here N is the noise signal and E is the field sampled at the receiver points, T is the total simulation time.

A few results are presented to illustrate how the reconstruction works with and without the noise in the measurement data. Figure 3.5 shows a reconstruction without noise. The permittivity reconstruction is almost perfect and conductivity reconstruction is also very good with only some small artifacts. In the presence of noise the reconstruction does not succeed as good. The reconstruction result with SNR=5 is presented in Figure 3.6. It is possible to recognize the object, however it's values are too low, and several artifacts can be seen, especially for the conductivity. A reconstruction from very noisy data (SNR=0.1) presented in Figure 3.7. No object is reconstructed, only artifacts are seen in the reconstruction.

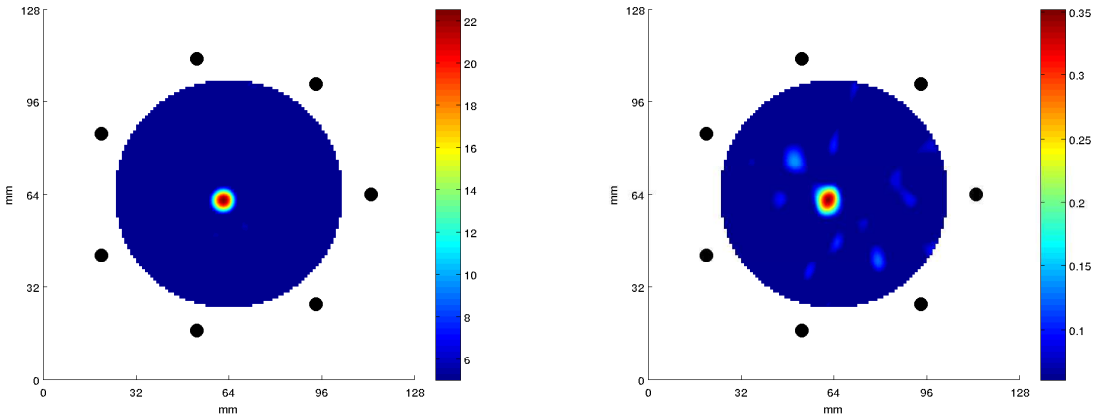

(a) Relative permittivity

(b) Conductivity

Figure 3.5: Reconstruction without noise

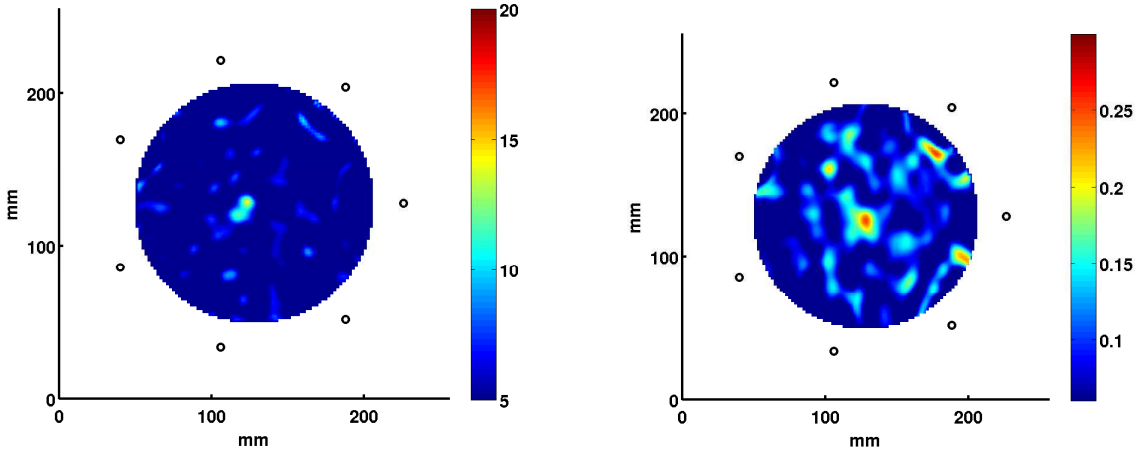

(a) Relative permittivity (b) Conductivity

Figure 3.6: Reconstruction from data with moderate amount of noise

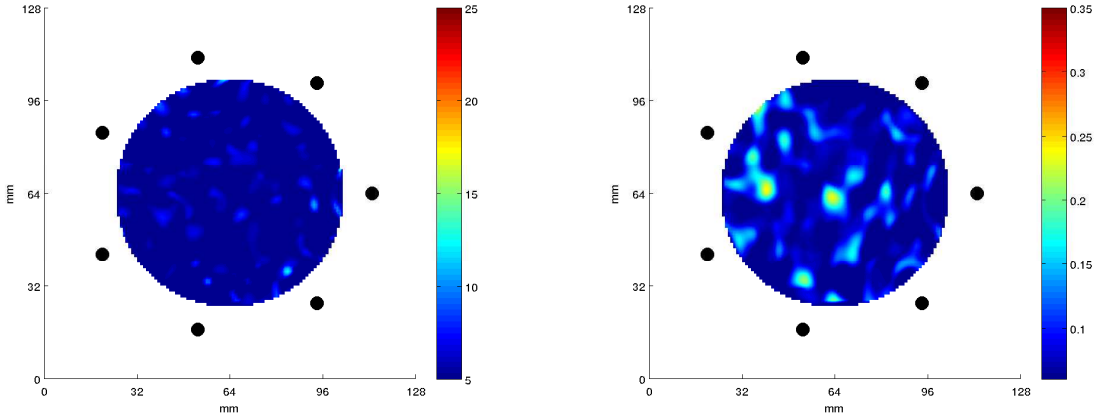

(a) Relative permittivity (b) Conductivity

Figure 3.7: Reconstruction from data with big amount of noise

3.3.3 Noise level and regularization

This group of experiments was made to determine how robust the reconstruction is to noise and how regularization can help to achieve stability of the solution and to improve the reconstruction. In this investigation only one reconstruction was done for each signal-to-noise ratio and regularization parameter. Since we add random noise, one reconstruction can't give us confident result, but can give some estimation for later investigations (see next section). Tikhonov and Edge preserving regularization with potential function φ_{GM} from Table 2.1 were used.

The results are plotted in three dimensions, that is the error measure is plotted as a function of the SNR and the regularization parameter. To plot 3D points in two dimensions it was chosen to linearly interpolate surface between points and draw surface colored according to the z-coordinate (error measure). Color bars are shown next to the plot itself. Actual points are marked with black. The color between these points is simply a result of an interpolation, no reconstructions were conducted there. Interpretation should be done carefully since one point can add a lot of "color" to the area around, and since there was only one reconstruction for every point, random values can heavily affect the final result.

The left column shows results for the relative permittivity reconstruction, and the right column for the conductivity reconstruction. The first line corresponds to reconstructions with Tikhonov regularization, and the second line to reconstruction with Edge-preserving regularization. On each plot the x-axis correspond to values of regularization parameter that is specific for the regularization scheme. This axis has a logarithmic scale. To the left the regularization parameter is smaller, that is it is closer to zero, and zero corresponds to no regularization. To the right regularization parameter is bigger, which refers to bigger amount of regularization applied during the reconstruction. Usually there exist optimal regularization parameter that gives the best reconstruction. With too big amount of regularization reconstruction is oversmoothed and it can lead to simply "flat" reconstruction since the object will be smoothed almost to the background level.

The Y-axis correspond to the noise level, SNR. Reconstructions are better for bigger SNR. For low SNR reconstruction usually fails, which will be shown in the error measures. Top corresponds to $SNR = 100$ and bottom corresponds to $SNR = 0.01$.

Figure 3.8 shows "Contrast" error measure defined in equation (3.4). A positive contrast says that at least one object value are bigger than the highest artifacts value, which means that reconstruction succeed. Negative contrast says that the level of artifacts are bigger than that of reconstructed object. Yellow and red color correspond to positive contrast, blue correspond to negative contrast. The general pattern is that for a low SNR the contrast is negative and for high SNR the contrast is positive. the borderline is around $SNR = 1$. We can see that with the Tikhonov regularization we can get a positive contrast for the conductivity for $SNR = 0.5$ with proper regularization while without regularization (or too small regularization) contrast is negative.

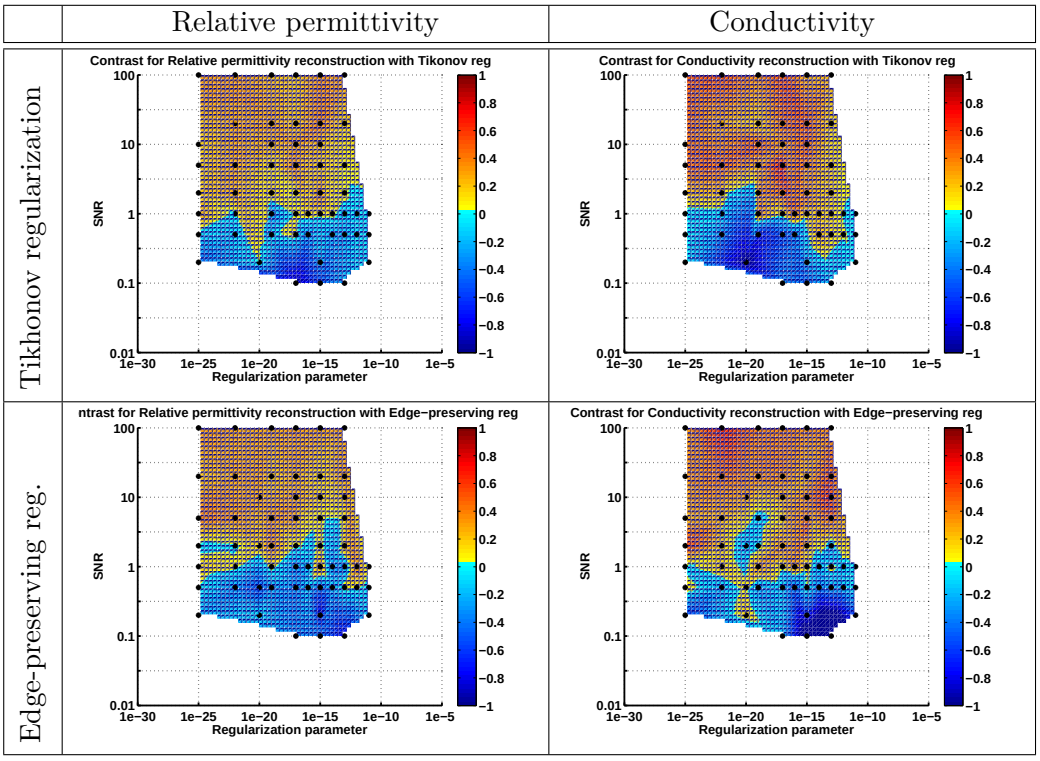

Figure 3.8: Contrast

Figure 3.9 shows the relative error, equation (3.1). The blue color corresponds to a good reconstruction with small relative error. Big relative error is marked with yellow and red and indicates a bad reconstruction. It is not a precise measure since it gives us good value even if reconstruction failed due to too big regularization (nothing is reconstructed except almost perfectly flat background). It can be clearly seen in the conductivity reconstruction. For a high SNR the relative error is usually small (blue) and for low SNR the reconstruction is bad (red).

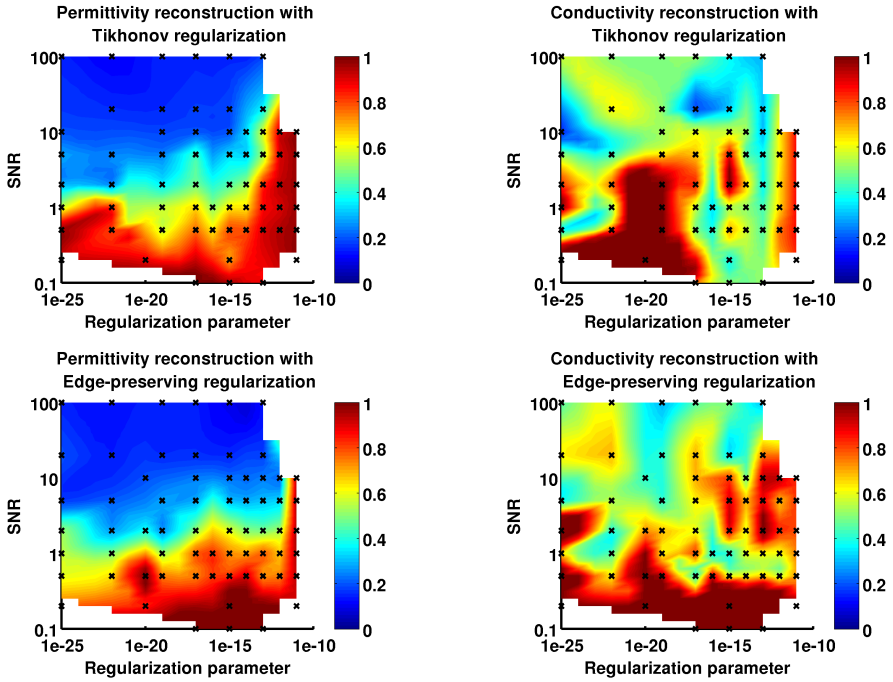

Figure 3.9: Relative error

To find out if the relative error is caused by a poorly reconstructed object or by high presence of the artifacts two measures Equations (3.2) and (3.3) are plotted on Figures 3.10 and 3.11. The relative error for the object shows that for a big regularization parameter ($\sim 10^{-11}$) the reconstruction is bad (red color) and the object is not reconstructed. The relative error for the artifacts with big regularization parameters in contrast are very small, that means no artifacts present in the reconstruction for the big regularization parameters.

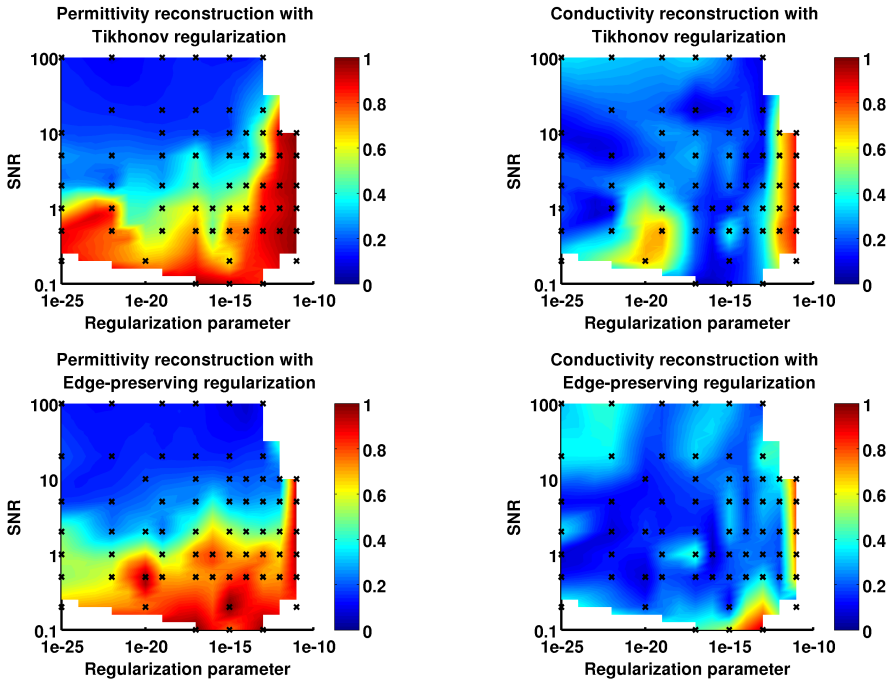

Figure 3.10: Relative error for object

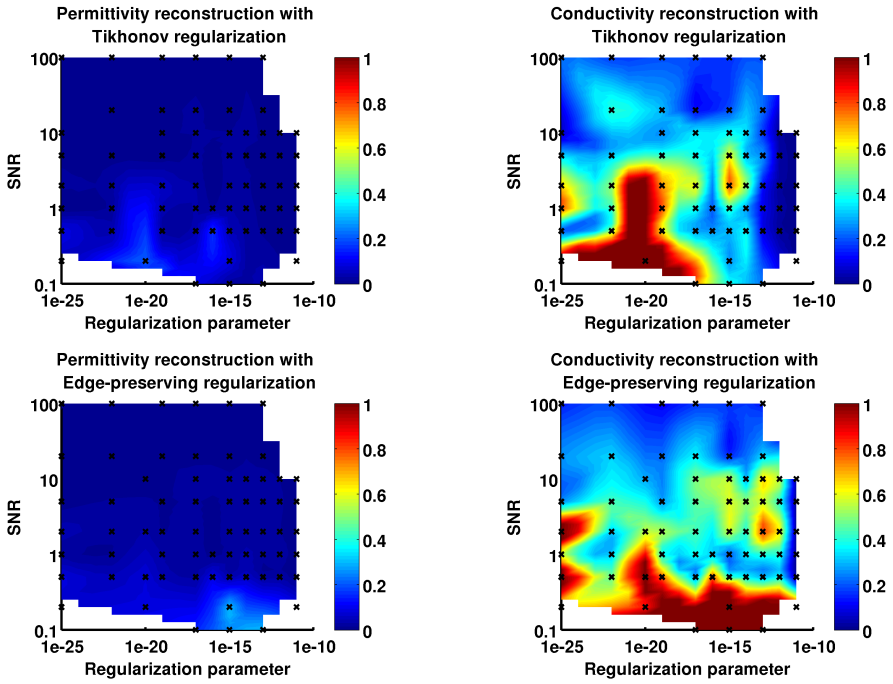

Figure 3.11: Relative error for artifacts

The relative maximal error for the whole reconstruction, as defined in equation (3.5), is shown in the Figure 3.12. Maximal error is smaller for permittivity reconstruction than for conductivity reconstruction. For big SNR the relative maximal error is small (blue).

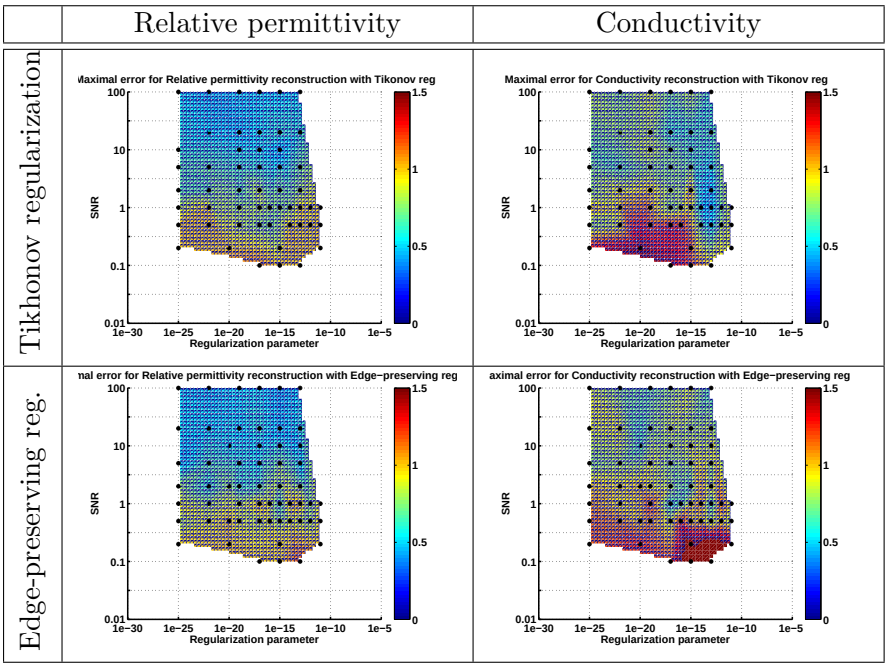

Figure 3.12: Maximal error

Only for those reconstructions where we got positive contrast and satisfactory all other error measures it is sensible to see what we have reconstructed. To see that, we try to fit object of known shape given in equation (3.6) (exactly the same as the original object, Table (3.1)) varying object's radius, height (foreground values), and position of it's center. This is done by least-squares minimization of the functions in equations (3.7) and (3.8). Sometime fitting fails due to the local minimas in the least-squares function or due to the big amount of artifacts in the reconstruction or due to the failed reconstruction (no object, only perfect background). In such cases fitted radius is very big or very small. Graphs should be treated carefully since one failed curve-fitting affects (colors) quite big area on the interpolated graph.

Figure 3.13 shows position where curve-fitting algorithm determines the object as defined in equation (3.12). When it is zero (blue color), position determined perfectly. As we can see, for high SNR the position is determined correctly all the time.

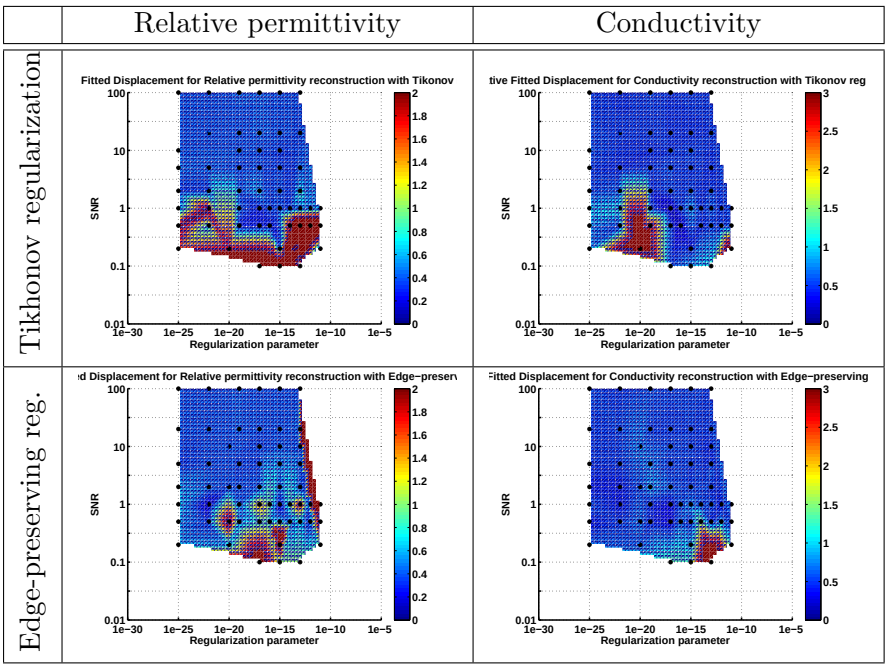

Figure 3.13: Displacement of the fitted object relative to the radius

Figure 3.14 shows foreground error measure value, the "height" of the fitted object, defined in the Equation (3.11). Green color corresponds to the good reconstruction. Blue indicates that reconstructed value is lower than the original and red indicates that the reconstructed value is bigger than the original. As we can see, for conductivity reconstructed values are sometimes bigger than original on good SNR. For relative permittivity values always smaller than original. For big regularization parameters for both

Tikhonov and Edge-preserving regularization "height" of fitted object is very small, it is very close to the background. The object is oversmoothed and is not reconstructed in such cases. This one more time shows the limit for the maximal regularization parameter value.

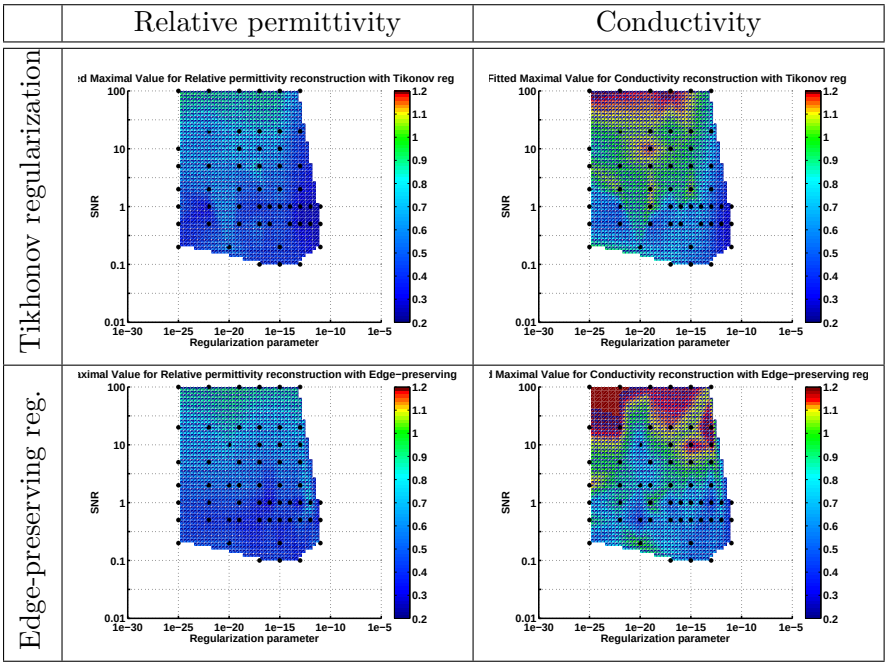

Figure 3.14: Fitted height value relative to original

Very important error measure for the regularizations comparison is the radius of fitted object. All other error measures are supplementary to ensure that the reconstruction succeeded. This measure shows if Edge-preserving regularization scheme performs better than previous Tikhonov regularization. Tikhonov regularization smoothes the object too much, that is why the radius is increased. The aim of the edge-preserving regularization is to achieve stability of the solution (we ensure that stability is achieved by previous error measures), but introduce less smoothness, thus keeping radius as close to the original as possible.

In the Figure 3.15 error measure for the fitted radius defined in the equation (3.10) is presented. The original radius $r_{orig} = 4$ cells, and for permittivity reconstruction in most cases it reconstructed correctly, which is shown with cyan color (see colormap). Red color says that reconstructed radius is bigger than original, dark blue - that fitted is smaller than original. For conductivity reconstruction fitted radius is almost always bigger than the original.

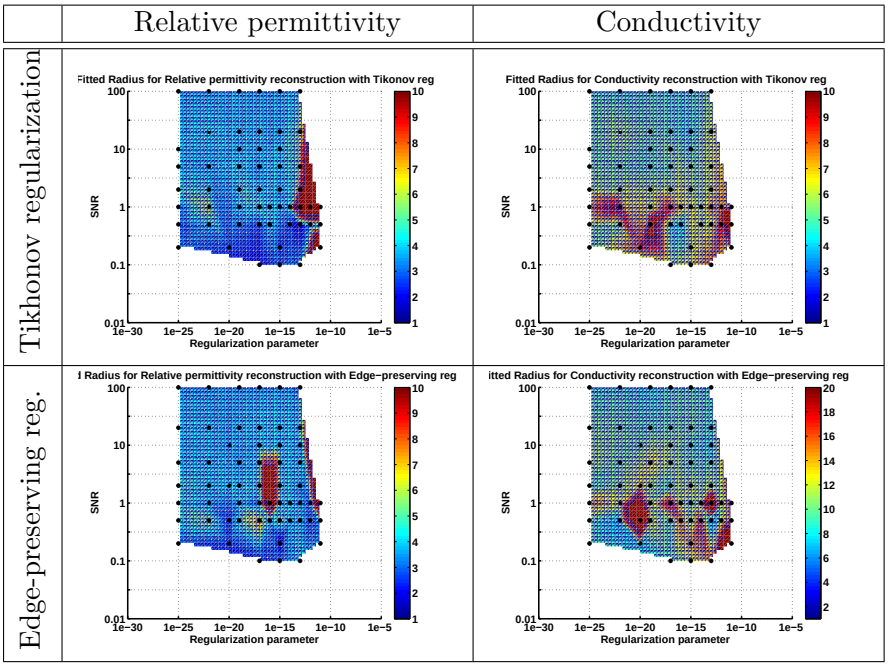

Figure 3.15: Fitted radius (original radius is 4)

Figure 3.15 shows that the radius of fitted object is in general smaller for edge-preserving regularization except for the one unusual point (relative permittivity reconstruction for the edge-preserving regularization with SNR 1 and regularization parameter 10^{-16}). All other error measures gives normal values for that point, that is why it is suspected that curve-fitting simply failed at this point due to the local minimum during the least squares minimization. To illustrate this particular case Figure 3.16 shows reconstructed relative permittivity and its central crossection. It is clearly seen that there is an object in the center and it is recognizable.

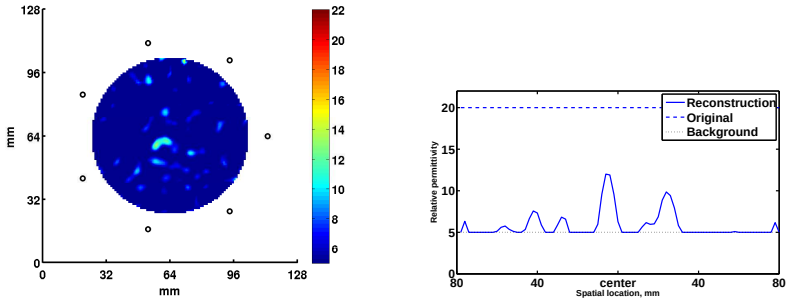

(a) Relative permittivity reconstruction

(b) Central cross-section

Figure 3.16: Relative permittivity reconstruction where curve-fitting failed

3.3.4 Statistics

We clearly can see that for SNR values higher than 10 the reconstruction always succeeds and there is no need for regularization. For $SNR < 1$ the reconstruction usually fails, it is not possible to reconstruct anything no matter if there is regularization or not. But for moderate SNR values we can benefit from regularization. With properly chosen regularization parameter we can get satisfactory reconstructions with regularization for cases where reconstructions without regularization fails or perform badly. Therefore a more detailed investigations with a smaller range of parameters has been done. Several SNR (10, 5, 2, 1, 0.5) and regularization parameters (1e-11, 1e-12, 1e-13, 1e-14, 1e-15, 1e-17) was used in a parameter studies. To enable a statistical analysis 4 simulations for each pair of parameters was made. For every pair the error measures defined in Section 3.2 was obtained. Then the mean value and standard deviation for each error measure was calculated.

Mean value is defined as

$$< x >= \frac{1}{N} \sum_{i=1}^{N} x_i$$

Standard deviation is defined as

$$\sigma^2 \sim \frac{1}{N-1} \sum_{i=1}^{N} (x_i - < x >)^2$$

From this statistical analysis we can make conclusions about the reconstruction quality and can estimate on average how good reconstruction we can expect for a particular SNR and regularization parameter.

In the following figures error measures are shown and their standard deviations. Each plot is made for a particular SNR that is written on the graph. The X-axis correspond to $\log_{10}$ of the regularization parameter. The values on the left are closer to zero and indicate a lower amount of regularization. Each graph contains values for the Tikhonov and for the Edge-preserving regularization. For higher SNR values the error measures indicate a better reconstructions.

Figure 3.17 shows the average contrast deduced from the 4 reconstructions for each set of parameters and it's standard deviation. Ideally contrast should be $\zeta_{contrast} = 1$, see definition in Equation (3.4). For high SNR values the contrast is positive, whereas for small SNR values it is negative. Figure 3.17 shows that there are satisfactory reconstructions where booth conductivity and relative permittivity are reconstructed with a positive contrast for $SNR \geq 2$.

As a result, for $SNR = 2$ a positive contrast is obtained in the reconstruction with proper amount of regularization, while reconstructions without regularization or too

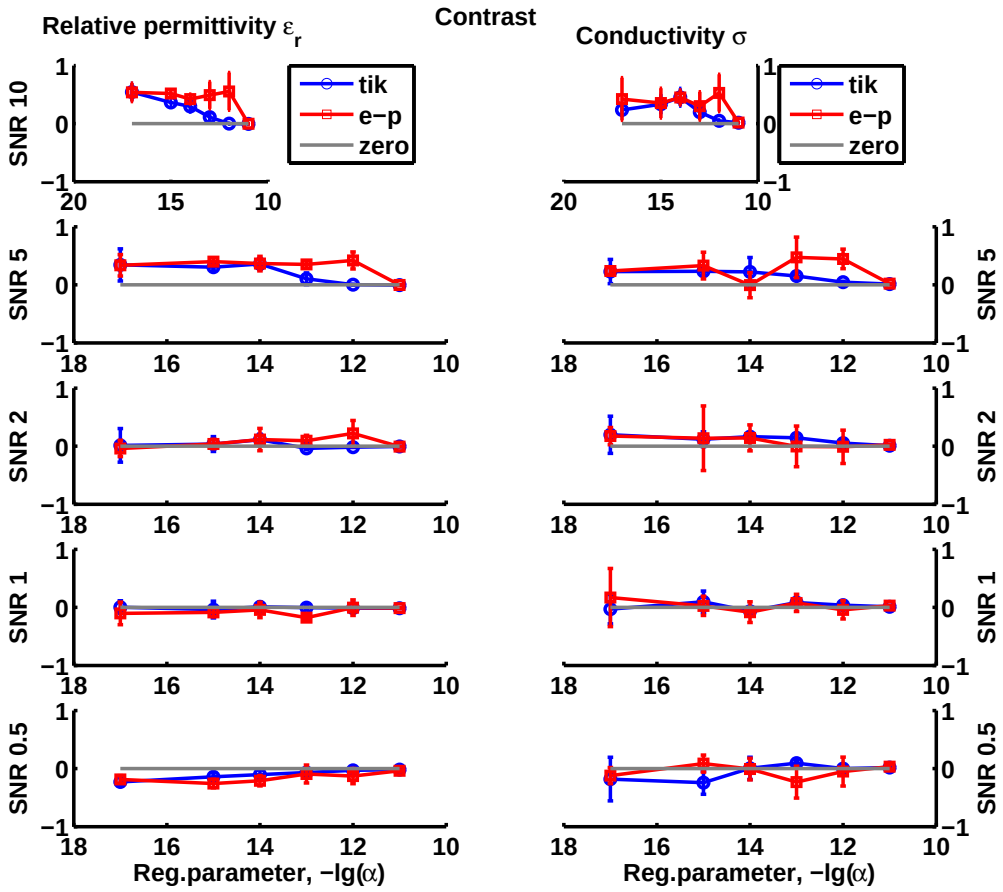

Figure 3.17: Contrast

weak regularization produce result with a negative contrast, that is artifacts are bigger than the object. For a low SNR regularization do not help since there is not enough data for a reconstruction. Tikhonov and Edge-Preserving regularizations achieve positive contrast on the same SNR range, when $SNR \geq 2$.

Figure 3.18 shows the relative error of the reconstructed image defined in Equation (3.1). For perfect reconstructions the relative error is 0. Figure shows that measure follows general pattern: error is smaller for bigger SNR.

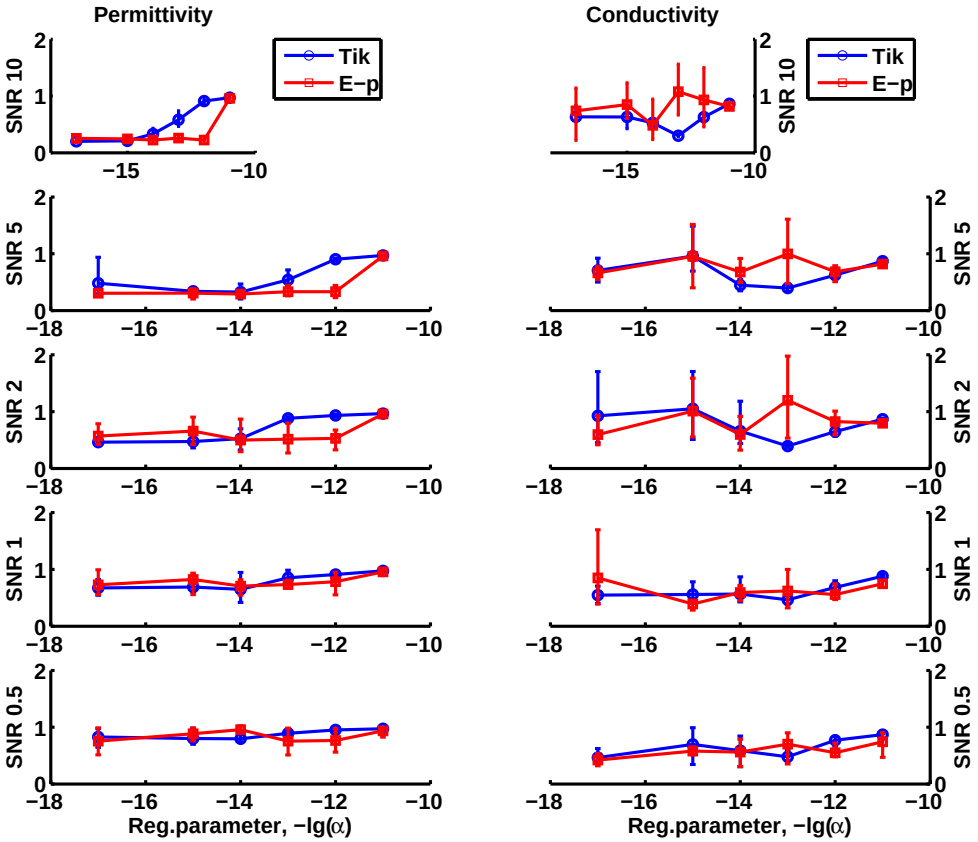

Figure 3.18: Relative error

Figure 3.19 shows the relative error for the object alone, without artifacts, defined in Equation (3.2). With a high regularization parameter this error measure clearly shows that the error in the object reconstruction is close to 1. This is due to an oversmoothed reconstruction where the object is not reconstructed at all.

Figure 3.20 shows the relative error for the artifacts defined in Equation (3.3). This measure shows that error due to artifacts is very small when reconstruction is oversmoothed.

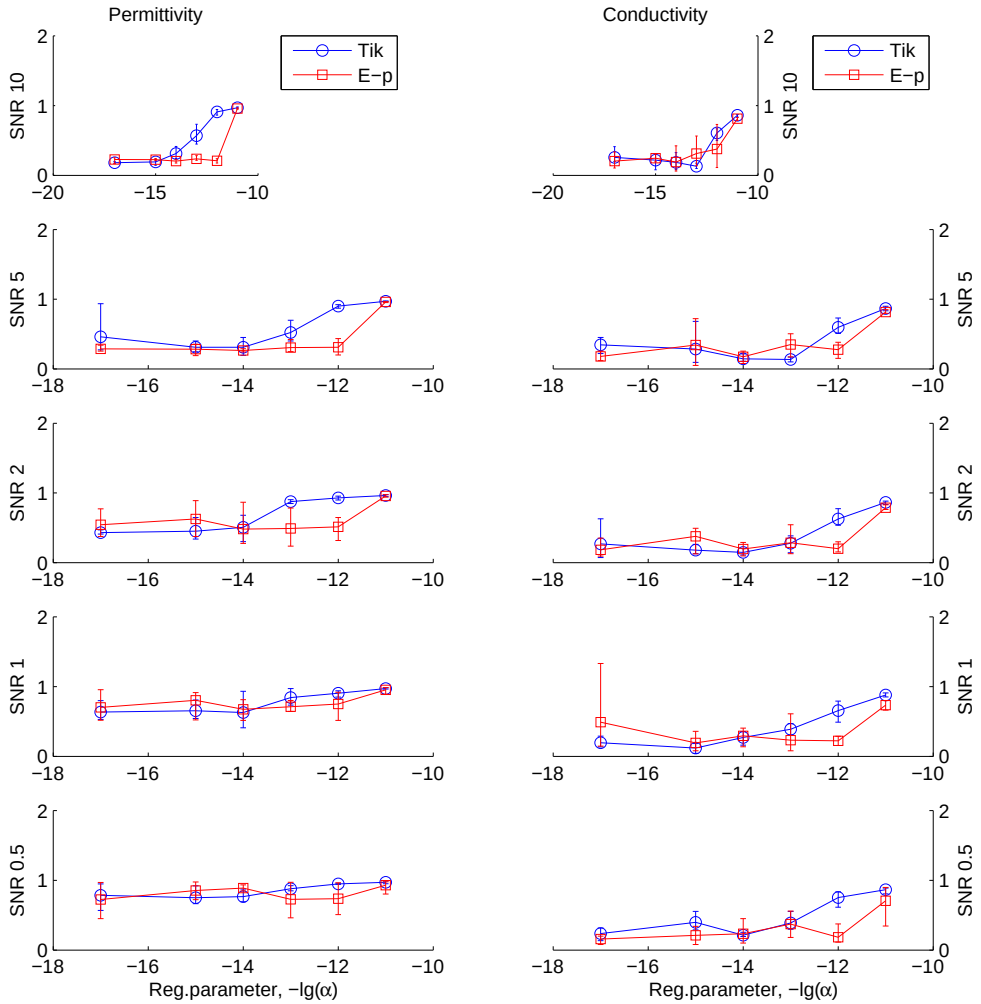

Figure 3.19: Relative error for object

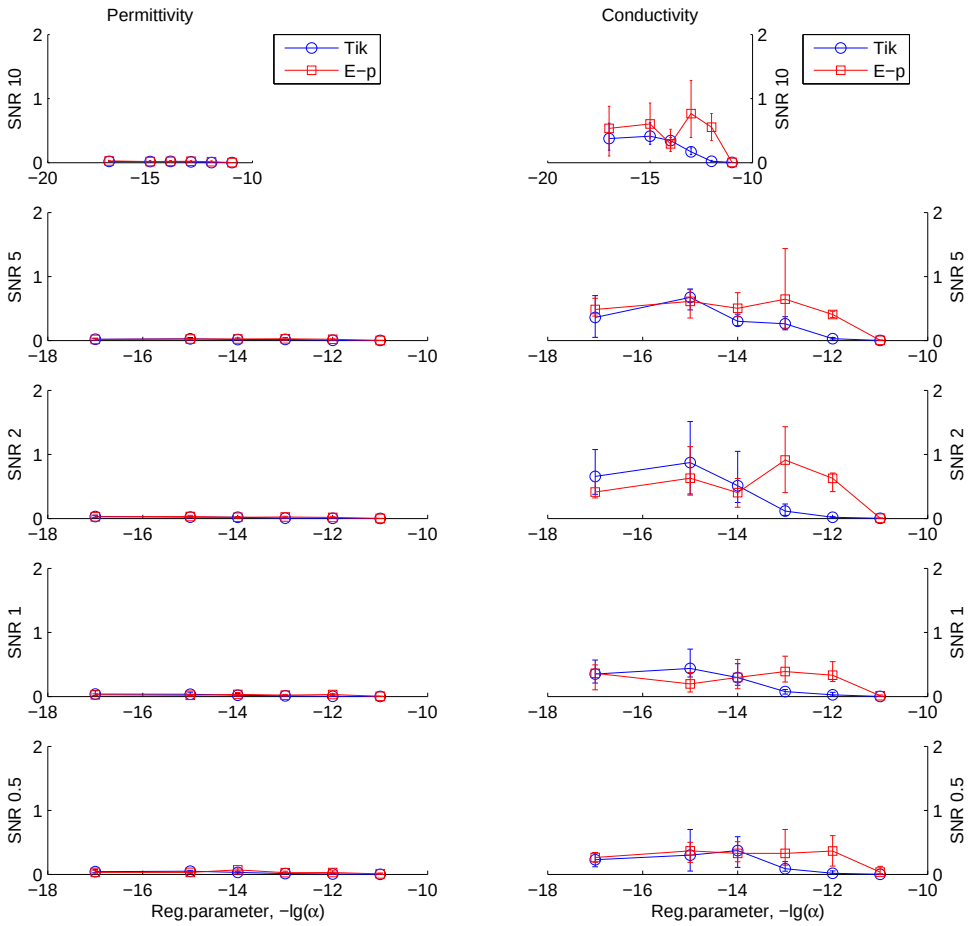

Figure 3.20: Relative error for artifacts

Figure 3.21 shows the relative misplacement of the reconstructed object defined in Equation (3.12). Ideally there should be no displacement. The line indicating displacement by the value of one original radius is shown to help visualize the displacement. For high SNR values the misplacement is small, less than one original radius. Starting from $SNR = 1$ misplacement become more, especially for permittivity reconstruction. Object displacement is smaller for the conductivity reconstruction due to chosen frequency.

Figure 3.22 shows "height" of the fitted object (maximum permittivity and conductivity value of the object as opposite to the background) as defined in Equation (3.11). For perfect reconstruction this value should be the same as original, 20 for relative permittivity and 0.24 Sm for conductivity (see Table (3.1)). For high regularization parameters it is close to the background value (5 for permittivity and 0.06 Sm for conductivity), which indicates that there was no object reconstructed. For smaller regularization parameters we can see bigger deviations in values due to the solution becoming unstable.

Figure 3.23 shows the radius of the object that could be best-fitted into reconstructed values as defined in Equation (3.10). Original radius for simulations is 4 grid cells, that should be for the perfect reconstruction. For Edge-preserving regularization, as expected, the radius is smaller. However, Tikhonov regularization gives satisfactory radius with small regularization parameters. We could use that, but with such small regularization parameters the relative error of the reconstruction increases. We should increase the regularization parameter to archive stability, and with increased parameters edge-preserving regularization gives a better result, that is radius is still small as for low regularization, but the stability is better as for a higher regularization.

With big regularization parameter (close to 10^{-11}) reconstructions are oversmoothed, and it it the reason why curve-fitting fails in that case. When curve-fitting failed radius and position of fitted object usually are too big, 5 times bigger than original.

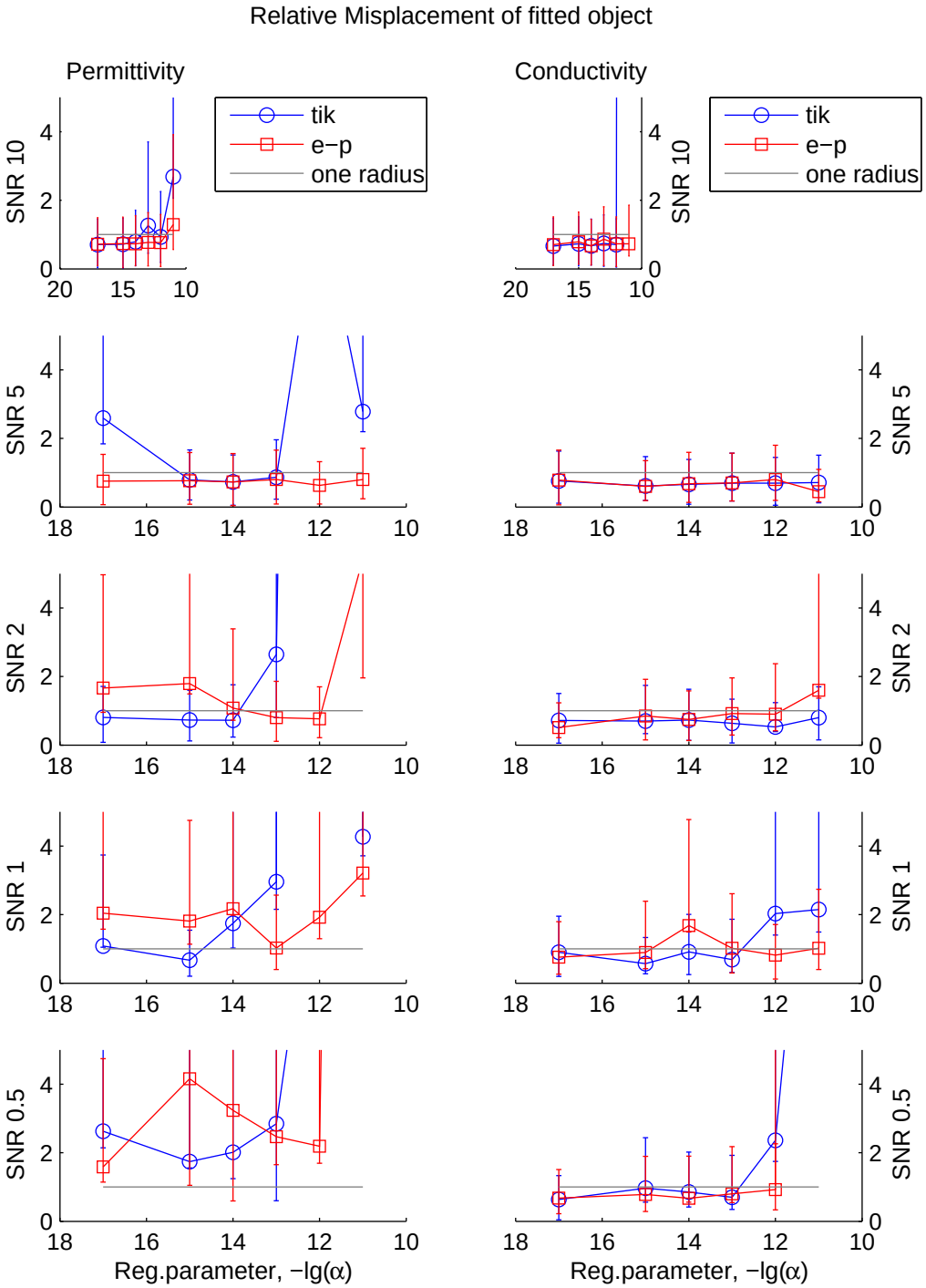

Figure 3.21: Relative misplacement of fitted object

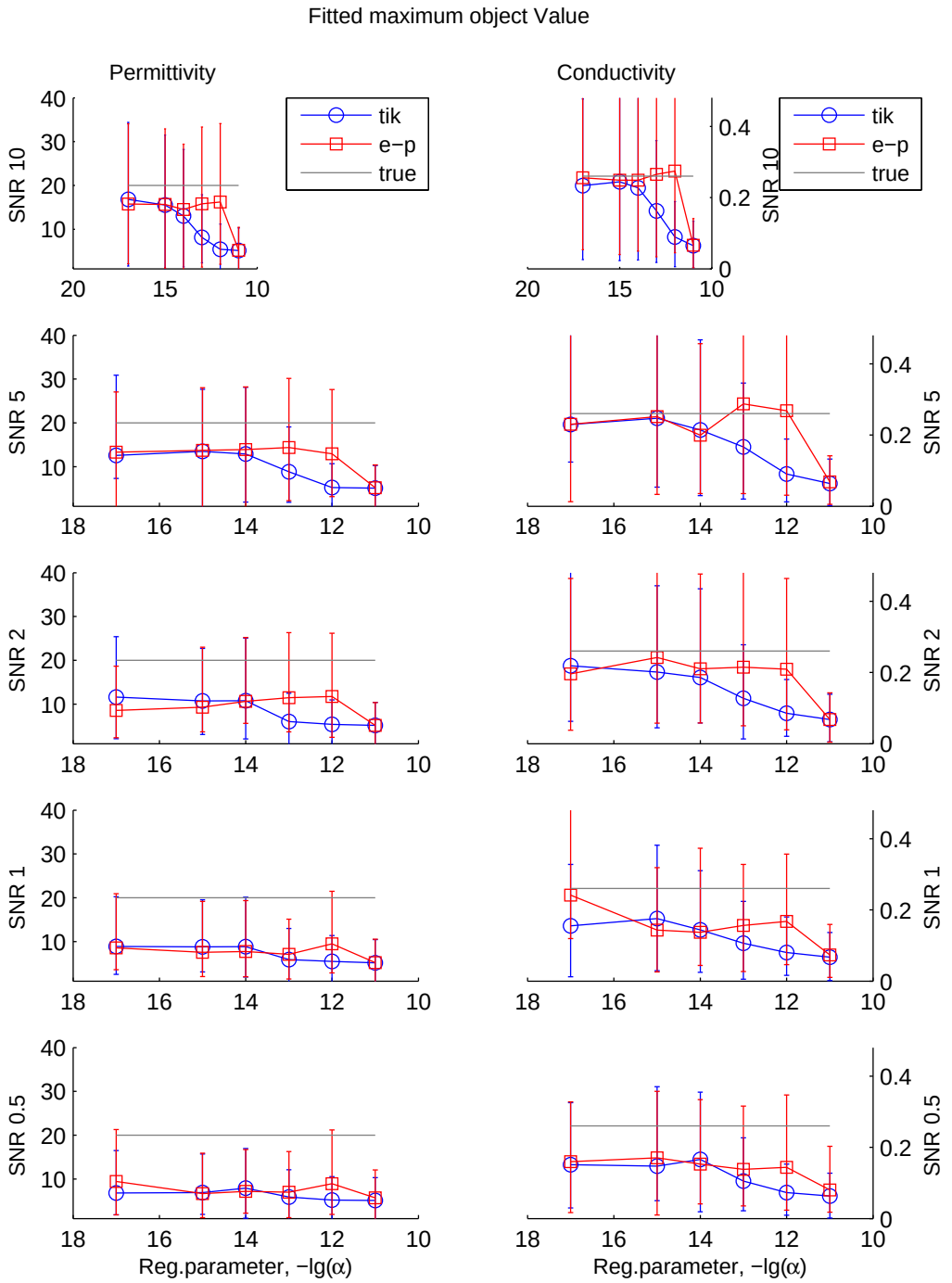

Figure 3.22: Height (foreground value) of fitted object

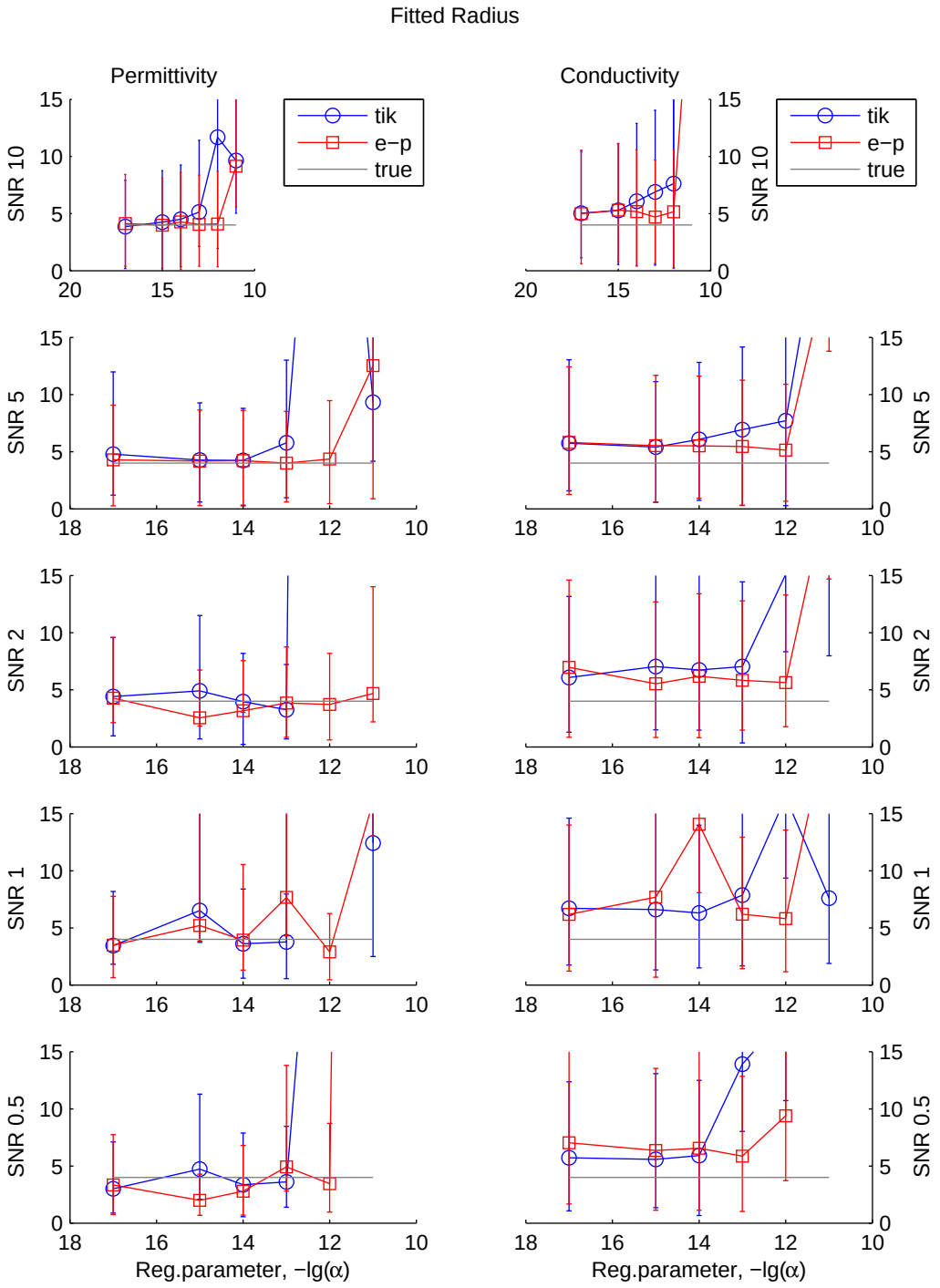

Figure 3.23: Fitted Radius (original 4)

4 Conclusions

Microwave tomography has a good potential to be used for the breast cancer imaging. There is a well-established FDTD method for simulation of the wave propagation, mature optimization methods. However, microwave tomography is an ill-posed inverse problem. This work provided more details about the regularization in order to cure the ill-posed inverse problem of tomography. Two regularization methods have been compared: Tikhonov regularization and Edge-preserving regularization.

It was found that the edge-preserving regularization does not perform very different from the Tikhonov regularization in conjunction with our particular reconstruction algorithm. It helps in cases with moderate amount of noise and gives wider range of regularization parameters without oversmoothing the solution compared to the Tikhonov regularization, but to get better results it might be necessary to use some other, more complex, potential functions. Such a function was described as a specialization of the generalized regularization. Important feature of edge-preserving regularization is that it gives edges of reconstructed object sharper comparing to Tikhonov regularization without introducing extra computational efforts. Edge-preserving regularization can not extend the SNR range where we can get satisfactory reconstructions. If SNR is an issue, improvement can be achieved by averaging among several measurements.

The more apriori information about the object we put into the regularization, the better the result. A new regularization will require more variables to determine. Now we search almost randomly for a good regularization parameter in a very wide range of values. If there will be more variables, it will take much more time to get a final reconstruction. Using automated methods for determination of regularization parameter, e.g. Generalized Cross-Validation, we can improve situation. With the edge-preserving regularization we get almost the same results.

From the algorithmic point of view future work is to use 3D FDTD method, Debye model of permittivity, implement Quasi-Newton optimization and automated procedure for determination of regularization parameter. In general, microwave tomography for breast cancer imaging is very promising method, but requires more investigations.

Bibliography

[1] "Cancer." World health organization, February 2006. Fact sheet.

[2] J. Michaelson, M. Silverstein, J. Wyatt, G. Weber, R. Moore, E. Halpern, D. Kopans, and K. Hughes, "Predicting the survival of patients with breast carcioma using tumor size," *Cancer*, vol. 95, pp. 713–723, 2002.

[3] C. Gabriel, S. Gabriel, and E. Corthout, "The dielectric properties of biological tissues: I. literature survey," *Physics in Medicine and Biology*, vol. 41, no. 11, pp. 2231–2249, 1996.

[4] S. Gabriel, R. W. Lau, and C. Gabriel, "The dielectric properties of biological tissues: II. measurements in the frequency range 10 hz to 20 ghz," *Physics in Medicine and Biology*, vol. 41, no. 11, pp. 2251–2269, 1996.

[5] S. Gabriel, R. W. Lau, and C. Gabriel, "The dielectric properties of biological tissues: III. parametric models for the dielectric spectrum of tissues," *Physics in Medicine and Biology*, vol. 41, no. 11, pp. 2271–2293, 1996.

[6] H. Fricke and S. Morse, "The electric capacity of tumors of the breast," *J. Caner Res*, vol. 10, p. 430, 1940.

[7] T. England and N. Sharples, "Dielectirc properties of the human body in the microwave region of the spectrum," *Nature*, vol. 163, pp. 487–480, 1949.

[8] T. England, "Dielectirc properties of the human body for wavelengths in the 1-10 cm range," *Nature*, vol. 166, pp. 480–481, 1950.

[9] J. Mallard and D. Lawn, "Dielectric absorbtion of microwaves in human tissues," *Nature*, vol. 213, pp. 28–30, 1967.

[10] J. Mallard and T. Whittingham, "Dielectric absorbtion of microwaves in human tissues," *Nature*, vol. 218, pp. 366–367, 1968.

[11] S. Chaudhary, R. Misha, A. Swarup, and J. Thomas, "Dielectric properties of normal and malignant human breast tissue at radiowave and microwave frequencies," *Indian J. Biochem. Biophys.*, vol. 21, pp. 76–79, 1984.

[12] J. Schepps and K. Foster, "The UHF and microwave dielectric properties of normal and tumour tissues: variation in dielectric properties with tissue water content," *Phys. Med. Biol.*, vol. 25, pp. 1149–1159, 1989.

[13] A. Surowiec, S. Stuchly, J. Barr, and A. Swarup, "Dielectric properties of breast carcinoma and the surrounding tissues," *IEEE Trans. Biomed. eng.*, vol. 35, pp. 257–263, 1988.

[14] W. Joines, Y. Zhang, C. Li, and R. Jirtle, "The measured electrical properties of normal and malignant human tissues from 50 to 900 mhz," *Med. Phys.*, vol. 21, pp. 547–550, 1994.

[15] A. Campbell and D. Land, "Dielectric properties of female human breast tissue measured in vitro at 3.2 ghz," *Phys. Med. Biol.*, vol. 37, pp. 193–210, 1992.

[16] A. Fhager, *Microwave Tomography*. PhD thesis, Chalmers University of Technology, 2006.

[17] W. Joines, "Frequency-dependent absorption of elctromagneic energy in biological tissue," *IEEE Trans. Biomed. Eng.*, vol. 25, pp. 17–20, 1984.

[18] P. Meaney, M. Fanning, D. Li, S. Poplack, and K. Paulsen, "A clinical prototype for active microwave imaging of the breast," *IEEE Trans. Microwave Theory Tech.*, vol. 48, pp. 1841–1853, 2000.

[19] D. Yoo, "The dielectric properties of cancerous tissues in a nude mouse xenograft model," *Bioelectromagnetics*, vol. 25, pp. 492–497, 1994.

[20] M. Bertero, M. Miyakawa, P. Boccacci, F. conte, K. Orikasa, and M. Furutani, "Image restoration in chirp-pulse microwave CT (CP-MCT)," *IEEE Trans. Biomed. Eng.*, vol. 47, pp. 690–699, 2000.

[21] A. Bulyshev, A. Souvorov, A. Semenov, R. Svenson, and G. Tatsis, "A computer simulation of three-dimensional microwave tomography," in *Engineering in Medicine and Biology society, 1997. Proceedings of the 19th Annual International Conference of the IEEE*, vol. 1, pp. 429–430, 1997.

[22] M. Gustafsson and S. He, "An optimization approach to two-dimensional time domain elecromagnetic inverse problems," *Radio and Science*, vol. 35, pp. 525–536, 2000.

[23] D. Colton and A. Kirsch, "A simple method for solving inverse scattering problems in the resonance region," *Inverse Problems*, vol. 12, no. 4, pp. 383–393, 1996.

[24] A. Fhager and M. Persson, "Comparison of two image reconstruction algorithms for microwave tomography," *Radio and Science*, vol. 40, 2005.

[25] A. Taflove and S. Hagnes, *Computational Electrodynamics: The Finite-Difference Time-Domain Method*. Artech House Publishers, 3-rd ed., 2005.

[26] M. Sadiku, *Numerical Techniques in Electromagnetics*. CRC Press, 2-nd ed., 2000.

[27] K. Kunz and R. Luebbers, *The Finite Difference Time Domain Method for Electromagnetics*. CRC Press, 1993.

[28] K. Yee, "Numerical solution of inital boundary value problems involving maxwell's equations in isotropic media," *Antennas and Propagation, IEEE Transactions on*, vol. 14, pp. 302–307, 1966.

[29] A. Taflove and M. Brodwin, "Numerical solutions of steady-state electromagnetic scattering problems using the time-dependent maxwell's equations," *IEEE Trans. Microwave Theory and Techniques*, vol. 23, pp. 888–896, 1975.

[30] J. Kraus, *Electromagnetics*. New York: McGraw-Hill, 3rd ed., 1984.

[31] P. Debye, *Polar molecules*. London: Dover Publications, 1929.

[32] K. S. Cole and R. H. Cole, "Dispersion and absorption in dielectrics i. alternation current characteristics," *J. Chem. Phys.*, vol. 9, p. 342, 1941.

[33] K. S. Cole and R. H. Cole, "Disperion and absorption in dielectrics ii. direct current characteristics," *J. Chem. Phys.*, vol. 10, p. 98, 1942.

[34] A. Tarantola, *Inverse Problem Theory and Model Parameter Estimation*. SIAM, 2005.

[35] M. Bertero and P. Boccacci, *Introduction to Inverse problems in imaging*. Bristol and Philadelphia: Institute of Physics Publishing, 1998.

[36] D. Colton and R. Kress, *Inverse Acoustic and Electromagnetic Scattering Theory*. New York: Springer-Verlag, 1992.

[37] V. Isakov, "Uniqueness and stability in multi-dimensional inverse problems," *Inv. Probl*, vol. 9, pp. 579–621, 1993.

[38] D. Colton and P. Paivarinta, "The uniqueness of a solution to an inverse scattering problem for electromagnetic waves," *Arch. Rational Mech. Anal.*, vol. 119, pp. 59–70, 1992.

[39] A. Tikhonov and V. Arsenin, *Solutions of ill-posed problem*. Winston, 1977.

[40] H. Carfantan and A. Mohammad-Djafari, "A bayesian approach for nonlinear inverse scattering tomographic imaging," in *Acoustics, Speech, and Signal Processing, International Conference on*, vol. 4, pp. 2311–2314, 1995.

[41] A. Baussard, D. Premel, and O. Venard, "A bayesian approach for solving inverse scattering from microwave laboratory-controlled data," *Inverse Problems*, vol. 17, pp. 1659–1669, 2001.

[42] J. Ye, C. Bouman, K. Webb, and R. Millane, "Nonlinear multigrid algoriths for bayesian optical difusion tomography," *IEEE Trans. on Image Processing*, vol. 10, pp. 909–922, 2001.

[43] G. Arfken, *Mathematical Methods for Physicists*. Academic Press, 3rd ed., 1985.

[44] J. Nocedal and S. Wright, *Numerical Optimization*. Springer, 1999.

[45] K. Levenberg, "A method for the solution of certain problems in least squares," *Quart. Appl. Math.*, vol. 2, pp. 164–168, 1944.

[46] D. Marquardt, "An algorithm for least-squares estimation of nonlinear parameters," *SIAM J. Appl. Math.*, vol. 11, pp. 431–441, 1963.

[47] J. Nocedal, "Updating quasi-newton matrices with limited storage," *Mathematics of Computation*, vol. 35, no. 151, pp. 773–782, 1980.

[48] M. Ulbrich, "A generalized tikhonov regularization for nonlinear inverse illposed problems," tech. rep., Techn. Univ. Munchen, June 1998.

[49] D. Strong and T. Chan, "Edge-preserving and scale-dependent properties of total variation regularization," *Inverse Problems*, vol. 19, no. 6, pp. S165–S187, 2003.

[50] C. Cohen-Bacrie, Y. Goussrd, and R. Guardo, "Regularized reconstruction in electrical impedance tomography using a variance uniformization constraint," *IEEE Transactions on Medical Imaging*, vol. 16, no. 5, pp. 562–571, 1997.

[51] T. Roths, M. Marth, J. Weese, and J. Honerkamp, "A generalized regularization method for nonlinear ill-posed problems enhanced for nonlinear regularization terms," *Computer Physics Communications*, vol. 139, pp. 279–296, 2001.

[52] R. Casanova, A. Silva, and A. R. Borges, "MIT image reconstruction based on edge-preserving regularization," *Physiological Measurement*, vol. 25, no. 1, pp. 195–207, 2004.

[53] H. Yoshida, T. Tanaka, and T. Takenaka, "Optimization approach with edge-preserving regularization to time domain 1d inverse scattering," *Electronics and Communications in Japan (Part II: Electronics)*, vol. 84, no. 10, pp. 1–8, 2001.

[54] P. Lobel, C. Picbota, L. Blanc-Feraud, and M. Barlaud, "Conjugate gradient algorithm with edge-preserving regularizationfor image reconstruction from experimental data," in *Antennas and Propagation Society International Symposium, 1996. AP-S. Digest*, vol. 39, pp. 12–14, 1996.

[55] P. Lobel, L. Blanc-Feraud, C. Pichot, and M. Barlaud, "Technical development for an edge-preserving regularization method in inverse scattering."

[56] P. Lobel, L. Blanc-Féraud, C. Pichot, and M. Barlaud, "A new regularization scheme for inverse scattering," *Inverse Problems*, vol. 13, no. 2, pp. 403–410, 1997.

[57] P. Charbonnier, L. Blanc-Feraud, and M. Barlaud, "An adaptive reconstruction method involving discontinuities," in *Acoustics, Speech, and Signal Processing, 1993. ICASSP-93., 1993 IEEE International Conference on*, vol. 5, pp. 491–494, 1993.

[58] P. Charbonnier, L. Blanc-Feraud, G. Aubert, and M. Barlaud, "Two deterministic half-quadratic regularization algorithms forcomputed imaging," in *Image Processing, 1994. Proceedings. ICIP-94., IEEE International Conference*, vol. 2, pp. 168–172, 1994.

[59] P. Charbonnier, L. Blanc-Féraud, G. Aubert, and M. Barlaud, "Deterministic edge-preserving regularization in computed imaging," *IEEE Transactions on image processing*, vol. 6, no. 2, pp. 298–311, 1997.

[60] M. Gustafsson, *Wave Splitting in Direct and Inverse Scattering Problems*. Lund University, 2000. this doctoral dissertation is a monograph.

[61] S. Geman and D. McClure, "Bayesian image analysis: An application to single photon emission tomography," in *Proc. Statistical Computation Section, Amer. Statistical Assoc.*, pp. 12–18, 1985.

[62] T. Hebert and R. Leahy, "Bayesian reconstructions from emission tomography data using a modified em algorithm," *IEEE Trans. Med. Imag.*, vol. MI-8, pp. 194–202, June 1990.

[63] G. Golub, M. Heath, and G. Wahba, "Generalized cross-validation as a method for choosing a good ridge parameter," *Technometrics*, vol. 21, pp. 215–223, 1979.

[64] G. Wahba, *Spline Models for Observational Data*, vol. 59 of *CBMS-NSF Regional Conference Series in Applied Mathematics*. Philadelphia: SIAM, 1990.

[65] P. C. Hansen, *Rank-Deficient and Discrete Ill-Posed Problems: Numerical Aspects of Linear Inversion*. SIAM, 1998.

[66] G. Mur, "Absorbing boundary conditions for the finite-difference approximation of the time-domain electromagnetic field equation," *IEEE Trans. Electromagn. Compat*, vol. EMC-23, no. 4, pp. 377–382, 1981.

[67] A. Fhager, P. Hashemzadeh, and M. Persson, "Reconstruction quality and spectral content of an electromagnetic time-domain inversion algorithm," *IEEE Trans. Biomedical Engineering*, pp. 1594–1604, 2006.